NRC Research Press

ARTICLE

Thermochronological constraints on the Eocene exhumation of the Grand Forks complex, British Columbia, based on $^{40}Ar/^{39}Ar$ and apatite fission track geochronology

J.F. Cubley, D.R.M. Pattison, D.A. Archibald, and M. Jolivet

Abstract: The Grand Forks complex (GFC) is a metamorphic core complex within the composite Shuswap complex in the southern Omineca belt of the Canadian Cordillera. It is juxtaposed against the surrounding low-grade rocks of the pericratonic Quesnel terrane by outward-dipping Eocene normal faults. The GFC attained peak metamorphic conditions of 750–800 °C and 5.5–6.0 kbar (1 kbar = 100 MPa) in the late Paleocene to early Eocene, followed by ~2.5 kbar of near-isothermal decompression at upper-amphibolite to granulite facies conditions (~725–750 °C) in the early Eocene. Subsequent low-temperature greenschist-facies exhumation (~0.7–1.5 kbar) was accommodated by the brittle–ductile Kettle River normal fault (KRF) on the east flank of the complex and the Granby fault (GF) on the west flank. This study presents 16 new $^{40}Ar/^{39}Ar$ hornblende and biotite dates from the GFC and low-grade rocks in the hanging walls to the KRF and GF. Cooling of the GFC through the closure temperature of hornblende (~ 530 °C) is constrained to the interval between ~54 and 51.4 ± 0.5 Ma, whereas cooling through the closure temperature of biotite (~280 °C) occurred at 51.4 ± 0.2 Ma. In the hanging wall of the KRF, cooling through the closure temperature of hornblende and biotite occurred nearly coevally at 51.7 ± 0.6 Ma and 51.0 ± 1.0 Ma, respectively. Five apatite fission track dates (closure temperature ~110 °C) from the GFC and adjacent hanging walls are indistinguishable within error, yielding an average age of 34.6 ± 2.0 Ma. The lack of difference in biotite and apatite ages between the GFC and the low-grade hanging wall rocks against which it is juxtaposed suggests no significant movement on the KRF and GF after ca. 51 Ma. Results from this study and a previous study on U–Pb dating of the GFC document rapid cooling of the GFC in excess of 200 °C/Ma in a 4 Ma interval between 55 and 51 Ma (Eocene). This rapid phase of exhumation of the GFC was followed by 15 Ma of slow cooling (~10 °C/Ma) of the joined GFC and hanging wall between ~280 °C (biotite closure) and ~110 °C (apatite closure).

Résumé : Le complexe de Grand Forks (GFC) est un complexe à noyau métamorphique à l'intérieur du complexe composite de Shuswap dans le sud de la ceinture Omineca de la cordillère canadienne. Il est juxtaposé aux roches environnantes, de faible métamorphisme, du terrane péricratonique de Quesnel par des failles normales à pendage vers l'extérieur, datant de l'Éocène. Le GFC a atteint des conditions métamorphiques de crête de 750–800 °C et de 5,5-6,0 kbar (1 kbar = 100 MPa) entre le Paléocène tardif et l'Éocène précoce; ces conditions ont été suivies d'une décompression quasi isotherme à ~2,5 kbar sous des conditions de faciès supérieur des amphibolites au faciès des granulites (~725–750 °C) à l'Éocène précoce. Par la suite, une exhumation à basse température, au faciès des schistes verts (~0,7–1,5 kbar), a été aidé par la faille normale cassante-ductile de Kettle River (KRF) sur le flanc est du complexe et par la faille Granby (GF) sur le flanc ouest. Cette étude présente 16 nouvelles datations $^{40}Ar/^{39}Ar$ sur une hornblende et une biotite du GFC et des roches à faible métamorphisme de l'éponte supérieure du KRF et du GR. Le refroidissement du GFC jusqu'à la température de fermeture de la hornblende (~530 °C) est limité à l'intervalle entre ~54 et 51,4 ± 0,5 Ma, alors que le refroidissement jusqu'à la température de fermeture de la biotite (~280 °C) a eu lieu il y a 51,4 ± 0,2 Ma. Dans l'éponte supérieure de la faille Kettle River, le refroidissement jusqu'à la température de fermeture de la hornblende et de la biotite s'est produit presque simultanément, soit respectivement à 51,7 ± 0,6 Ma et 51,0 ± 1,0 Ma. Cinq datations obtenues par traces de fission sur l'apatite (température de fermeture ~110 °C) provenant du GFC et des épontes supérieures adjacentes sont indistinguables à l'intérieur de la marge d'erreur, donnant une moyenne de 34,6 ± 2,0 Ma. Le manque de différence dans les âges de la biotite et de l'apatite entre le GFC et les épontes supérieures des roches à faible métamorphisme auxquelles ils sont juxtaposés suggèrerait qu'aucun mouvement significatif ne s'est produit le long de la faille Kettle River et la faille Grangy après 51 Ma. Selon les résultats de la présente étude et d'une étude antérieure portant sur la datation U–Pb du GFC, un refroidissement rapide du GFC à plus de 200 °C/Ma serait survenu dans un intervalle de 4 Ma entre 55 et 51 Ma (Éocène). Cette phase rapide d'exhumation du GFC a été suivie de 15 Ma de refroidissement lent (~10 °C/Ma) de l'ensemble GFC et l'éponte supérieure entre ~280 °C (fermeture de la biotite) et ~110 °C (fermeture de l'apatite). [Traduit par la Rédaction]

Introduction

The Grand Forks complex (GFC) is a north–south-trending, fault-bounded metamorphic core complex straddling the border between southern British Columbia and northern Washington State (Fig. 1). It is known as the Kettle dome or Kettle complex south of the US–Canada border (e.g., Cheney 1980; Orr and Cheney 1987; Mulch et al. 2007; Kruckenberg et al. 2008). The GFC is one of a number of core complexes within the composite Shuswap complex of the southern Omineca belt (e.g., Pigage 1977; Brown and Read 1983; Okulitch 1984; Brown and Journeay 1987), which represents the hinterland to the Cordilleran orogenic belt (Fig. 1) (e.g., Monger et al. 1982; Coney and Harms 1984; Simony and Carr 2011).

Received 21 March 2012. Accepted 19 October 2012.

Paper handled by Associate Editor Marc St-Onge.

J.F. Cubley* and D.R.M. Pattison. Department of Geoscience, University of Calgary, 2500 University Drive NW, Calgary, AB T2N 0A8, Canada.
D.A. Archibald. Department of Geological Sciences and Geological Engineering, Miller Hall, Queen's University, Kingston, ON K7L 3N6, Canada.
M. Jolivet. Géosciences Rennes, UMR 6118, Université de Rennes 1, Campus de Beaulieu, 35042 Rennes Cedex, France.
Corresponding author: J.F. Cubley (e-mail: jcubley@yukoncollege.yk.ca).
*Present address: School of Mining and Technology, Yukon College, 500 College Drive, Whitehorse, YT Y1A 5K4, Canada.

Fig. 1. Regional map of the southeastern Canadian Cordillera adapted from Glombick et al. (2006) and Wheeler and McFeely (1991). Western Canada map from Johnson and Brown (1996). AB, Alberta; BC, British Columbia; BF, Beaven fault; CAN, Canada; CF, Cherry–Cherryville fault; CRF, Columbia River fault; FC, Frenchman Cap dome; GF, Granby fault; GFC, Grand Forks complex; GHF, Gallagher fault; GRF, Greenwood fault; HF, Hope fault; KRF, Kettle River fault; MD, Monashee décollement; NA, North America; NF, Newport fault; OD, Okanogan dome; OVF, Okanagan Valley fault; PRC, Priest River complex; PTF, Purcell Trench fault; SCF, Standfast Creek fault; SD, Spokane dome; SLF, Slocan Lake fault; SLTZ, Shuswap Lake transfer zone; TO, Thor–Odin dome; VC, Valhalla complex; VG, Vaseaux gneiss; VSZ, Valkyr shear zone.

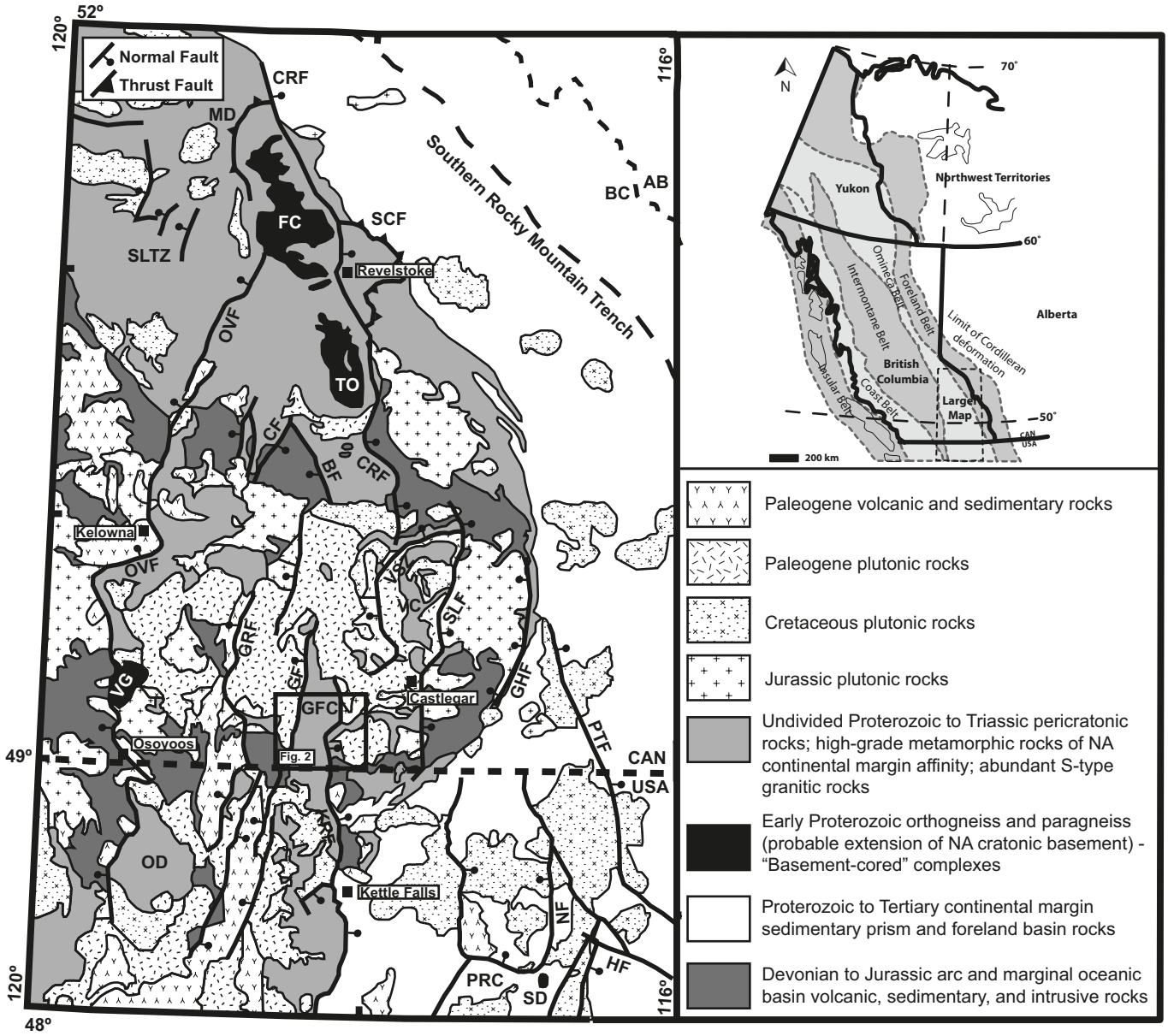

The rocks within the complex are Paleoproterozoic to Paleozoic metasedimentary rocks of the Grand Forks Group, metamorphosed to middle amphibolite to granulite facies conditions (Fig. 2) (Laberge and Pattison 2007; Cubley 2012; Cubley and Pattison 2012). This high-grade metasedimentary package is juxtaposed against low-grade transitional greenschist–amphibolite facies metasedimentary, metavolcanic, and metaintrusive rocks across the Kettle River fault (KRF) on the eastern flank and Granby fault (GF) on the western flank (Höy and Jackaman 2005*a*, 2005*b*; Laberge and Pattison 2007; Cubley and Pattison 2012).

The mechanisms, rates, and thermal implications of core complex exhumation have been the focus of much recent study, both in the Cordillera and elsewhere (e.g., Gessner et al. 2007; Rey et al. 2009; Malavieille 2010). Thermomechanical modelling of the Shuswap complex by Rey et al. (2009) proposed a "fast extension" model for regional exhumation in the Eocene, characterized by rapid exhumation at amphibolite facies conditions and then rapid cooling following decompression. Field-based tectonics research in the Shuswap complex has largely been conducted using the lens of such thermomechanical models, focusing on determining the timing of Eocene exhumation in the region (e.g., Teyssier et al. 2005; Hinchey et al. 2007; Gordon et al. 2008; Kruckenberg et al. 2008; Simony and Carr 2011) and constraining the rate of subsequent cooling of core complexes at higher structural levels (e.g., Lorencak et al. 2001; Vanderhaeghe et al. 2003; Gordon et al. 2008; Hallett and Spear 2011). A key component of our understanding of core complex exhumation has been the increasingly widespread recognition of two distinct stages of exhumation: an early stage at

Fig. 2. Bedrock geology and geochronology of the 082E/01 Grand Forks 1:50 000 map sheet, adapted from Höy and Jackaman (2005*b*). (A) Bedrock geology and first-order structural features. (B) Compilation of pre-existing U–Pb monazite (Mnz) and $^{40}Ar/^{40}K$ hornblende and biotite data. Monazite ages are the youngest Eocene age populations. Previous geochronology from 1, Addie (1980); 2, Baadsgaard et al. (1961); 3, Cubley et al. (2013); 4, Armstrong et al. (1991); 5, Stevens et al. (1982); 6, Wanless et al. (1968); 7, Hunt and Roddick (1990); 8, Getty Mines Ltd. (unpublished data); 9, Wanless et al. (1979); 10, Laberge and Pattison (2007); 11, Stevens et al. (1983). (C) New $^{40}Ar/^{39}Ar$ hornblende, $^{40}Ar/^{39}Ar$ biotite, and apatite fission track (AFT) dates from this study. See Tables 2–4 for summary hornblende, biotite, and apatite results, respectively. Act, actinolite; Bt, biotite; Grt, garnet; Hbl, hornblende; HW, hanging wall; Pl, plagioclase; SZ, shear zone.

high temperatures (granulite to upper-amphibolite facies conditions), closely followed by a second stage at lower temperatures (primarily greenschist facies conditions) (e.g., Simony and Carr 1997; Norlander et al. 2002; Vanderhaeghe et al. 2003; Hinchey et al. 2006; Mulch et al. 2007; Kruckenberg and Whitney 2011).

Until recently, the GFC had undergone less detailed study than other core complexes in the southern Shuswap complex — e.g., the Valhalla complex (Carr et al. 1987; Parrish et al. 1988; Spear and Parrish 1996; Simony and Carr 1997; Schaubs et al. 2002; Spear 2004; Carr and Simony 2006; Fig. 1). Primary bedrock mapping was conducted in the late 1960s by Preto (1970). Laberge and Pattison (2007) and Cubley and Pattison (2012) conducted petrological studies of the GFC, the surrounding low-grade rocks, and the bounding normal faults (GF and KRF). Peak metamorphic conditions of 750–800 °C and 5.5–6 kbar (1 kbar = 100 MPa) were inferred for migmatitic sillimanite + garnet + K-feldspar pelitic gneisses of the GFC, corresponding to depths of 19–21 km based on an average crustal density of 2.85 g/cm^3 (Laberge and Pattison 2007; Cubley and Pattison 2012). Microtextural evidence suggests an episode of high-temperature (high-*T*; ~725–750 °C) decompression following peak metamorphism, resulting in exhumation to 3–4 kbar (~10–14 km depth) (Laberge and Pattison 2007; Cubley and Pattison 2012). This was followed by further low-temperature (low-*T*) greenschist facies extension and exhumation on the KRF and GF (Laberge and Pattison 2007; Mulch et al. 2007; Cubley and Pattison 2012; Cubley et al. 2013).

A study by Cubley et al. (2013) on monazite and zircon U–Pb geochronology from the GFC constrained peak metamorphism to 58–50 Ma and suggested that high-*T* decompression occurred at 52–50 Ma. This high-*T* decompression thus occurred just prior to greenschist facies brittle–ductile deformation on the KRF at ~49 Ma (Berger and Snee 1992; Mulch et al. 2007). The juxtaposition of these high- and low-*T* decompression events requires a cooling rate of >100 °C/Ma between ~52 and 49 Ma, in contrast to the slower cooling rate of 25 °C/Ma inferred by Laberge and Pattison (2007). The interpretation of Cubley et al. (2013) is consistent with previously reported $^{40}Ar/^{40}K$ biotite dates from the GFC (52–49 Ma; Wanless et al. 1968, 1979; Addie 1980; Stevens et al. 1983) but is inconsistent with previously reported 64–60 Ma $^{40}Ar/^{40}K$ hornblende ages (Stevens et al. 1982; Hunt and Roddick 1990), the latter of which underpinned the slower cooling rate of Laberge and Pattison (2007).

This study attempts to better constrain the timing and rate of cooling of the GFC following the high-*T* segment of its exhumation and to resolve some of the above discrepancies. It complements studies by Laberge and Pattison (2007), Cubley and Pattison (2012), and Cubley et al. (2013) that describe the petrological and high-*T* geochronological history of the area. New $^{40}Ar/^{39}Ar$ hornblende, $^{40}Ar/^{39}Ar$ biotite, and apatite fission track (AFT) dates are presented to help constrain the low-*T* portion of the GFC cooling history. The results allow refinement of the cooling history of the GFC and its hanging wall rocks.

Regional geology

The GFC forms a broad, north–south-trending structural dome that plunges shallowly to the south, exposing stratigraphically deeper levels in British Columbia than those observed to the south in Washington State (Preto 1970; Cheney 1980; Orr and Cheney 1987). The GFC is composed primarily of the Grand Forks Group (Preto 1970; Höy and Jackaman 2005*a*), a mixed Paleoproterozoic to lower Paleozoic metasedimentary succession comprising pelitic schists and gneisses, amphibolites, marbles, calcsilicates, and quartzites. The predominant lithology observed within the complex is migmatitic Sil + Bt + Kfs ± Grt (Sil, sillimanite; Bt, biotite; Kfs, K-feldspar; Grt, garnet) pelitic paragneiss (mineral abbreviations after Kretz (1983)). This succession was intruded by a suite of Proterozoic to lower Paleozoic intrusives that were metamorphosed and coevally deformed with the metasedimentary rocks, producing granitic to tonalitic orthogneisses (Preto 1970; Armstrong et al. 1991; Ross and Parrish 1991; Höy and Jackaman 2005*a*).

Metamorphic grade in the GFC decreases in the southwestern part of the map area (Fig. 2A), where higher structural and stratigraphic levels (units Pr4 and Pr5) are juxtaposed against lower units (Pr1 and Pr3) across poorly constrained faults. Upper amphibolite to granulite facies conditions are documented within Sil + Kfs ± Grt paragneisses and Hbl ± Cpx ± Opx (Hbl, hornblende; Cpx, clinopyroxene; Opx, orthopyroxene) amphibolites of the lower units (Pr1 and Pr3), whereas middle-amphibolite conditions characterized by St + Bt ± Sil (St, staurolite) and Grt + Bt schists are observed west of the town of Grand Forks (Unit Pr5) (Preto 1970; Cubley and Pattison 2012). In the higher-grade migmatitic paragneisses, Crd + Spl + Ilm ± Rt (Crd, cordierite; Spl, spinel; Ilm, ilmenite; Rt, rutile) reaction textures around sillimanite and Crd + Qtz (Qtz, quartz) coronas around garnet imply high-*T* (~725–750 °C), near-isothermal decompression from 5.5–6 kbar (20–22 km) (peak regional metamorphism) to 3.2–4.2 kbar (11–15 km) (Laberge and Pattison 2007; Cubley and Pattison 2012). The mechanism for this high-*T* exhumation is not well understood, but exhumation is proposed to have occurred at ~52–50 Ma based on in situ dating of monazite within decompression reaction textures and on crosscutting field relationships (Cubley et al. 2013). Local metre-scale shear zones that postdate the development of primary gneissosity (S2) are observed throughout the complex, typically with top-to-the-east kinematic indicators. These shear zones are folded by a number of high-*T* folding episodes (F3a,b) that are in turn truncated by ~50 Ma Eocene granitoid bodies across the width of the complex (Cubley and Pattison 2012). The high-*T* exhumation segment was followed by a post-50 Ma episode of low-*T* greenschist facies exhumation accommodated by the GF and KRF (Laberge and Pattison 2007; Cubley and Pattison 2012; Cubley et al. 2013).

A limited number of pre-existing $^{40}Ar/^{40}K$ hornblende and biotite dates from the western margin of the complex (Fig. 2B) suggest passage through hornblende closure temperature (~530 ± 30 °C; Harrison 1981) at ~64–60 Ma (Stevens et al. 1982; Hunt and Roddick 1990), followed by passage through biotite closure (~280 ± 40 °C, Harrison et al. 1985) at 52–49 Ma (Wanless et al. 1968, 1979; Addie 1980; Stevens et al. 1983). These dates imply slow cooling (~25 °C/Ma) following high-*T* decompression, an interpretation that is at odds with a number of observations and models for cooling elsewhere within the Shuswap complex that document rapid cooling to greenschist facies conditions (e.g., Gibson et al. 1999; Vanderhaeghe et al. 2003; Glombick et al. 2006; Hinchey et al. 2007; Kruckenberg et al. 2008; Rey et al. 2009). In addition, the $^{40}Ar/^{40}K$ dates at ~64–60 Ma contradict monazite ages for peak metamorphism (58–50 Ma) and high-*T* decompression (52–50 Ma) (Cubley et al. 2013).

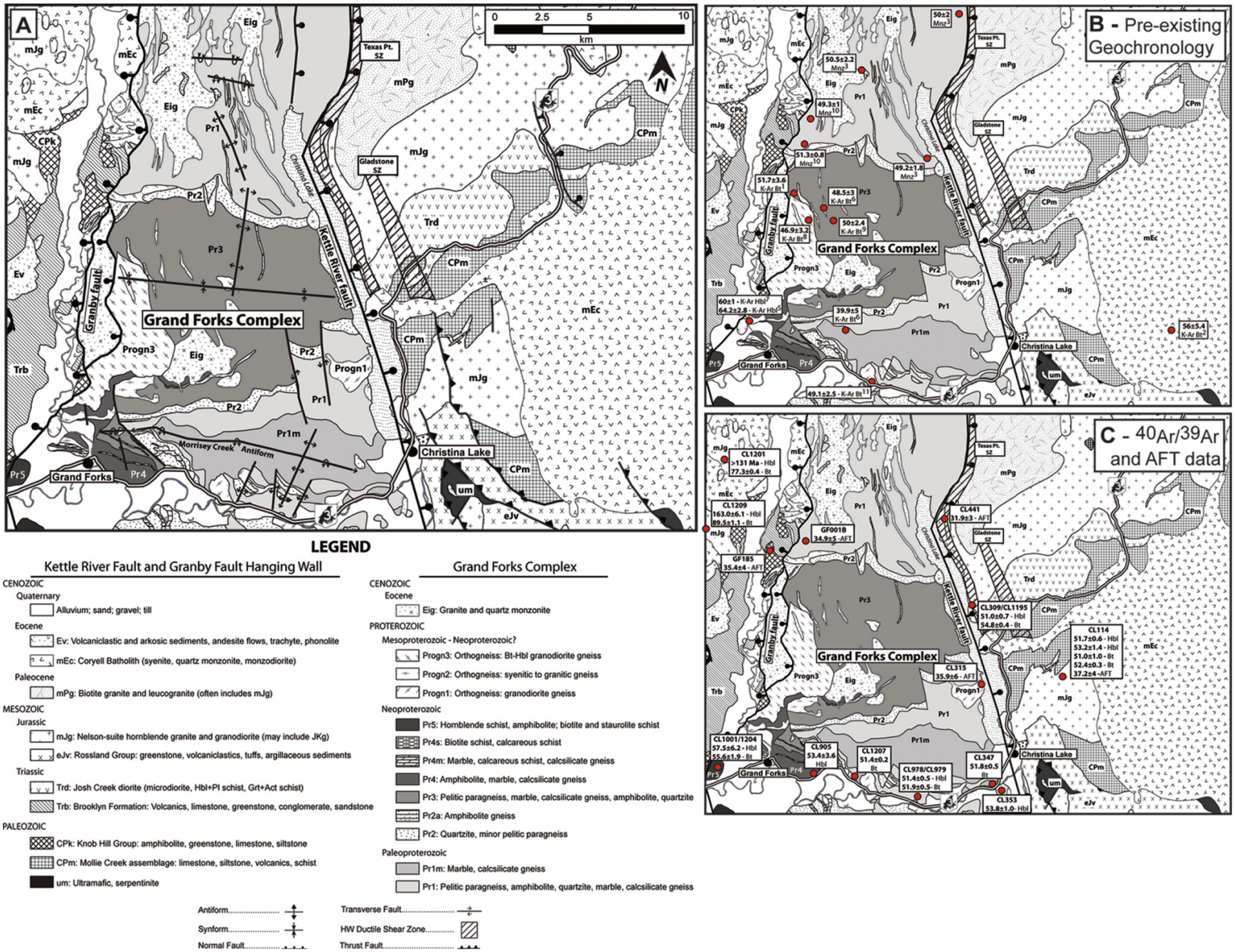

The eastern margin of the GFC is defined by the east-dipping KRF (Figs. 1, 2). In northeast Washington, the fault is a brittle–ductile greenschist facies extensional system that was active at ~49 Ma (Rhodes and Cheney 1981; Orr and Cheney 1987; Berger and Snee 1992; Mulch et al. 2007). In the deeper stratigraphic levels exposed in British Columbia, the footwall mylonitic foliation attributed to the KRF in Washington is not developed, and brittle deformation fabrics associated with the fault cut high-*T* footwall gneisses at a high angle (Rhodes and Cheney 1981; Cubley and Pattison 2012). Variable brittle deformation of hanging wall rocks extends at least 300 m from the presumed fault trace (Cubley and Pattison 2009).

Juxtaposed across the fault are low-grade Carboniferous to early Jurassic sedimentary, volcanic, and volcaniclastic rocks of the Mollie Creek Assemblage and Rossland Group (Fig. 2) (Acton 1998; Acton et al. 2002; Höy and Jackaman 2005*a*; Cubley and Pattison 2012). These rocks constitute part of the pericratonic Quesnel terrane that was obducted onto the North American craton in the Middle Jurassic (Erdmer et al. 2001; Unterschutz et al. 2002). The hanging wall stratigraphy is intruded by numerous plutonic suites, including the ~216 Ma Josh Creek diorite (Acton et al. 2002), the 167.9 ± 1.3 Ma Nelson granitoid suite (Cubley et al. 2013), the 59.5 ± 0.53 Ma Ladybird leucogranite suite (Cubley et al. 2013), and the 51.1 ± 0.5 Ma Coryell alkaline suite (Carr and Parkinson 1989). Peak burial metamorphism in the KRF hanging wall reached transitional greenschist–amphibolite facies conditions (~425 ± 25 °C) in the Early to Middle Jurassic, prior to the intrusion of the Nelson granitoid suite (Acton et al. 2002; Höy 2006; Cubley and Pattison 2012). Contact metamorphism related to the Nelson suite locally produced Crd + Kfs-bearing migmatites (Cubley and Pattison 2009, 2012). The vertical displacement attributed to the low-*T* KRF is 2.5–2.8 km (0.7–0.8 kbar) (Cubley and Pattison 2009, 2012). The latest deformation postdated the emplacement of Coryell suite intrusives (Parrish et al. 1988; Acton 1998; Cubley and Pattison 2012).

In the immediate hanging wall of the KRF is a normal-sense ductile shear zone, the Texas Point shear zone (TPSZ), which can be traced from the Texas Point area north along the KRF trace (Fig. 2). The degree of ductile strain within the TPSZ is highly variable, and undeformed ~59 Ma leucogranite bodies within the shear zone suggest that the emplacement of leucogranites may have outlasted TPSZ deformation (Cubley et al. 2013). Movement along this shallow to moderately east-dipping shear zone is constrained to between 59 and 51 Ma, and it is truncated by undeformed Coryell suite intrusives (Cubley et al. 2013). The TPSZ is therefore temporally distinct from the brittle KRF. Because the TPSZ forms the boundary between the GFC and hanging wall rocks northeast of Christina Lake, it has been tentatively linked to the early, high-*T* (amphibolite facies) segment of GFC exhumation (Cubley et al. 2013). If all high-*T* exhumation of the GFC is attributed to the TPSZ, it accommodates a vertical displacement of ~8 km (2.3 kbar); however, given its limited exposure and variable degree of strain, questions remain about its relative contribution to overall exhumation.

The GFC is bounded on its western margin by the GF, a predominantly brittle, variably west-dipping listric normal fault (Carr and Parkinson 1989; Fyles 1990; Laberge and Pattison 2007). South of the border in Washington State, the GF forms the eastern margin of the Republic graben, a syn-extensional rift basin (Suydam and Gaylord 1997). The GF juxtaposes GFC high-grade rocks against a succession of Quesnel metasedimentary and volcanic rocks broadly similar to that in the hanging wall of the KRF but comprising different late Paleozoic to Triassic stratigraphic units (Acton et al. 2002; Cubley and Pattison 2009). The Middle Jurassic Nelson suite and Eocene Coryell intrusions in the hanging wall of the KRF are also observed in the hanging wall of the GF. Similar to the KRF hanging wall, burial metamorphism reached transitional greenschist–amphibolite facies conditions (~425 ± 40 °C), the timing of which is not well constrained (Laberge and Pattison 2007). Brittle movement on the GF postdated the intrusion of 51.1 ± 0.5 Ma Coryell suite alkalic intrusives, and the associated crush zone is observed up to 230 m from the fault (Carr and Parkinson 1989; Laberge and Pattison 2007). The vertical displacement attributed to the low-*T* movement on the GF is 1.5 ± 1 kbar or 5 ± 3.5 km, similar to that inferred for the KRF, with a westward dip estimated at 25–35° (Carr and Parkinson 1989; Laberge and Pattison 2007).

Geochronology sample descriptions

Sixteen $^{40}Ar/^{39}Ar$ (8 Hbl, 8 Bt) and five AFT samples were selected for isotopic analysis. $^{40}Ar/^{39}Ar$ sampling in the GFC was conducted on an east–west transect along Highway 3 (Fig. 2), enabling sampling from multiple stratigraphic levels (Pr1, Pr4, and Pr5) at a relatively constant elevation. Hanging wall $^{40}Ar/^{39}Ar$ samples were collected from coarse-grained Jurassic Nelson suite rocks, as the fine grain size of hanging wall metasedimentary and metavolcanic rocks precluded effective mineral separation. Hornblende and biotite sample pairs in the hanging walls to the GF and KRF came from either (*i*) the same rock sample or (*ii*) two outcrops in close proximity. The locations of all samples are shown in Fig. 2C, with Universal Transverse Mercator (UTM) location data for all samples presented in Table 1. Abbreviated descriptions of the samples are given below.

GFC

GFC hornblende samples

Sample CL353 is a Hbl + Pl + Qtz + Ilm + Ttn + Ap (Pl, plagioclase; Ttn, titanite; Ap, apatite) amphibolite gneiss from unit Pr1, the basal sedimentary unit of the GFC (Fig. 3A). It is located on the southeastern margin of the GFC in the immediate footwall of the KRF (Fig. 2C). The amphibolite is intruded by weakly foliated to unfoliated Hbl–Bt granite correlative with unit Progn1 (Orr and Cheney 1987; Höy and Jackaman 2005*b*). Both amphibolite and granite locally show brittle deformation features (cataclasis, Chl ± Ep veining (Chl, chlorite; Ep, epidote)) attributed to the KRF, but the sample in question appears unaltered both in hand sample and thin section. Hornblende grains record microprobe Ca/K ratios of 10–12 (Appendices 1, 3)[1].

Sample CL978 is a Hbl + Bt + Pl + Qtz + Ilm + Rt + Ap + Ttn amphibolite gneiss also from unit Pr1 (Fig. 2C). The amphibolite gneiss forms a volumetrically small portion of an outcrop that also includes Sil + Grt + Bt migmatitic paragneiss, quartzofeldspathic psammitic gneiss, and minor quartzite. This complex package of gneissic lithologies is strongly folded (Fig. 3B). Though generally unaltered, a small number hornblende grains (Ca/K = 5.8–7.3) contain biotite inclusions up to 30 μm × 100 μm, as well as limited chlorite growth parallel to cleavage planes.

Sample CL905 is a strongly foliated amphibolite schist from unit Pr4, collected from a roadside outcrop along Highway 3 east of the village of Grand Forks (Fig. 2). The sample has a Hbl + Bt + Pl + Qtz + Ilm + Ttn ± Ep ± Grt assemblage, with minor retrograde chloritization of hornblende as <20 μm lamellae parallel to cleavage planes. Microprobe Ca/K ratios range from 12.5 to 14.5.

Sample CL1204 is a fine-grained Hbl + Pl + Qtz + Mt + Ilm (Mt, magnetite) amphibolite schist from unit Pr5, the uppermost GFC unit exposed in British Columbia, west of the village of Grand Forks (Fig. 2). This rusty schist shows a well-developed foliation overprinted by minor, late alteration attributed to the nearby GF. This alteration is characterized by ~0.5 mm Cal + Ep (Cal, calcite) veining with local

[1]Supplementary data are available with the article through the journal Web site at http://nrcresearchpress.com/doi/suppl/10.1139/cjes-2012-0058.

Table 1. Locations and sample descriptions of $^{40}Ar/^{39}Ar$ and AFT samples.

Sample no.	Location	Unit	Easting	Northing	Altitude (ft)	Mineral(s) analyzed
CL114	KRF hanging wall: edge of Nelson intrusion east of Christina Lake	mJg	415452	5438039	3157	Hbl, Bt, Ap
CL309	KRF hanging wall: mylonitic Nelson granitoid in southern TPSZ, eastern shore of Christina Lake	mJg	408889	5442747	1614	Bt
CL315	GFC: hornblende granodiorite at southwestern end of Christina Lake	Progn1	409676	5436648	1585	Ap
CL347	GFC: Grt + Bt + Crd paragneiss south of Christina Lake	Pr1	410770	5430599	1659	Bt
CL353	GFC: Hbl + Pl amphibolite gneiss south of Christina Lake	Pr1	411507	5429963	1594	Hbl
CL441	KRF hanging wall: mylonitic Nelson granitoid in TPSZ at northeastern end of Christina Lake	mJg	406695	5449107	2045	Ap
CL905	GFC: Hbl + Bt amphibolite schist east of Grand Forks	Pr4	398183	5431207	1782	Hbl
CL978	GFC: Hbl + Bt amphibolite gneiss southwest of Christina Lake	Pr1	405168	5429468	2087	Bt
CL979	GFC: Sil + Bt + Crd migmatitic paragneiss southwest of Christina Lake	Pr1	405514	5429331	1939	Hbl
CL1001	GFC: St + Bt + Sil pelitic schist west of Grand Forks	Pr5	391491	5431809	2275	Bt
CL1195	KRF hanging wall: lineated Hbl-granite tectonite in southern TPSZ, eastern shore of Christina Lake	mJg	408866	5442860	1618	Hbl
CL1204	GFC: Hbl + Bt amphibolite schist west of Grand Forks	Pr5	391696	5431968	1884	Hbl
CL1207	GFC: Grt + Bt paragneiss between Grand Forks and Christina Lake on Highway 3	Pr1	400791	5430925	2164	Bt
GF001B	GFC: Quartz monzonite dike on the western margin of the core complex	Eig	397544	5446542	3170	Ap
GF186	GF hanging wall: Bt-syenite dike (Coryell suite)	mEc	395370	5446036	2503	Ap

Notes: 1 ft = 0.3048 m. All UTM coordinates are NAD83, Zone 11. Unit abbreviations correspond to those in Fig. 2.

chloritization of fine-grained hornblende. Hornblende in the majority of the rock is coarser grained and shows little replacement, limited to ≤15 μm lamellar biotite intergrowths in a small number of grains. These relatively unaltered grains (Ca/K = 27–35) were targeted during mineral separation.

GFC biotite samples

Sample CL347 is a Grt + Bt + Crd + Pl + Qtz ± Kfs ± Sil paragneiss collected from unit Pr1 along the eastern margin of the GFC south of Christina Lake (Figs. 2, 3D). Nearby Di + Bt (Di, diopside) calc-silicate gneisses (unit Pr1 m) show an early, top-to-the-east mylonitic foliation that has been subsequently folded during D3a deformation (see Fig. 4C, Cubley et al. 2013). There is local minor replacement of biotite by Chl + Rt, but biotite is generally unaltered.

Sample CL979 is a Sil + Bt + Crd + Kfs + Pl + Qtz + Ilm migmatitic paragneiss from unit Pr1 (Fig. 2). Chlorite replacement of biotite in this sample is variable, with zones of pristine biotite within migmatite leucosomes but chloritized biotite elsewhere in the thin section. Samples CL347 and CL979 display Crd + Qtz coronae around garnet and Crd + Ilm ± Spl coronae around sillimanite, reflecting high-*T* decompression at amphibolite facies conditions (Laberge and Pattison 2007; Cubley and Pattison 2012).

Sample CL1207 is a quartzofeldspathic Kfs + Bt + Pl + Qtz + Ilm paragneiss from unit Pr1, located halfway between the GF and KRF (Fig. 2). The strongly foliated paragneiss is interlayered with lenses of Di-bearing calc-silicate gneiss. Alteration is limited, with only minor chloritization of biotite and local sericitization of plagioclase.

Sample CL1001 is a St + Bt + Pl + Qtz + Ilm + Sil + Grp + Mt (Grp, graphite) pelitic schist from Unit Pr5 of the GFC, collected west of Grand Forks in the immediate footwall of the GF (Fig. 2), but it exhibits no textural evidence for brittle deformation. This rusty, graphite-rich schist is fine-grained and strongly foliated, with latest foliation development postdating development of the peak metamorphic assemblage. Alteration of biotite is not evident in thin section, but BSE and microprobe analyses of biotite suggest local chloritization.

GFC apatite samples

Sample CL315 is a weakly foliated hornblende granodiorite from intrusive unit Progn1 on the southwestern shore of Christina Lake (Fig. 2). The sample locality also contains post-kinematic Eocene biotite leucogranite and more strongly deformed Progn1 biotite orthogneiss. Sample GF001B was collected from a quartz monzonite dike hosted in Sil + Grt + Kfs paragneiss of unit Pr1, located on the western margin of the GFC in the Volcanic Creek area (Fig. 2; Laberge 2005). The emplacement of the dike postdates development of S2 gneissosity and local high-strain zones in the host paragneisses and is correlated with the ~50 Ma post-kinematic Eocene granitoid suite documented by Cubley et al. (2013).

KRF hanging wall samples

KRF hornblende samples

Sample CL114 is a hornblende–biotite granodiorite from the Sutherland Creek drainage east of Christina Lake (Fig. 2). This granodiorite yielded a U–Pb zircon date of 167.9 ± 1.3 Ma (Cubley et al. 2013), indicating that it belongs to the regionally extensive Middle Jurassic Nelson granitoid suite. The medium-grained Hbl + Bt + Pl + Kfs + Qtz + Ap granodiorite is weakly to moderately foliated. Hornblende, biotite, and apatite were all separated from sample CL114. Petrographic analysis of hornblende grains shows rare <25 μm lamellar chlorite intergrowths along cleavage planes, with microprobe Ca/K ratios ranging from 9 to 10. Biotite grains similarly show limited replacement by chlorite intergrowths concentrated along the {001} cleavage plane.

Sample CL1195 is a Hbl + Pl + Kfs + Qtz + Ilm + Ttn + Ap granodiorite correlated with the Nelson granitoid suite and located within the TPSZ on the northeastern edge of Christina Lake (Fig. 2) (Cubley and Pattison 2012; Cubley et al. 2013). The sample itself is minimally deformed, with no evidence of significant matrix recrystallization and (or) mineral alteration related either to the TPSZ or subsequent brittle overprinting by the KRF. The sample is lineated with large, east-trending hornblende crystals and Hbl ± Ttn aggregates (3f). Hornblende grains are pristine, with very rare <25 μm chlorite intergrowths and Ca/K ratios ranging from 5.5 to 6.5.

KRF biotite samples

Sample CL309 is a ductilely deformed, coarse-grained Bt + Pl + Kfs + Qtz orthogneiss from the TPSZ, collected ~25 m south of hornblende sample CL1195 (Fig. 3G). It is correlative with the 167.9 ± 1.3 Ma (Cubley et al. 2013) Nelson intrusive suite based on lithologic similarity (Acton 1998; Cubley and Pattison 2012). Biotite grains within the sample show no alteration, and there is no visible brittle deformation overprint from the KRF. The gneiss is

Fig. 3. Representative field photographs of dated lithologies. Sample locations are shown in Fig. 2C. (A) CL353: strongly foliated Hbl-amphibolite, GFC. (B) CL978: deformed Sil + Grt + Kfs + Bt migmatitic paragneiss, GFC. (C) CL905: fine-grained Hbl + Bt amphibolite schist, GFC. (D) CL347: Bt ± Sil quartzofeldspathic paragneiss, GFC. (E) CL1003: rusty Sil + St + Bt schist west of Grand Forks (CL1001 locality), GFC. (F) CL1195: lineated Nelson suite granodiorite with elongate hornblende grains, KRF hanging wall. (G) CL309: Nelson suite Bt-granodiorite orthogneiss in the TPSZ along eastern shore of Christina Lake, KRF hanging wall. (H) CL186: coarse-grained Coryell suite syenite dike, GF hanging wall.

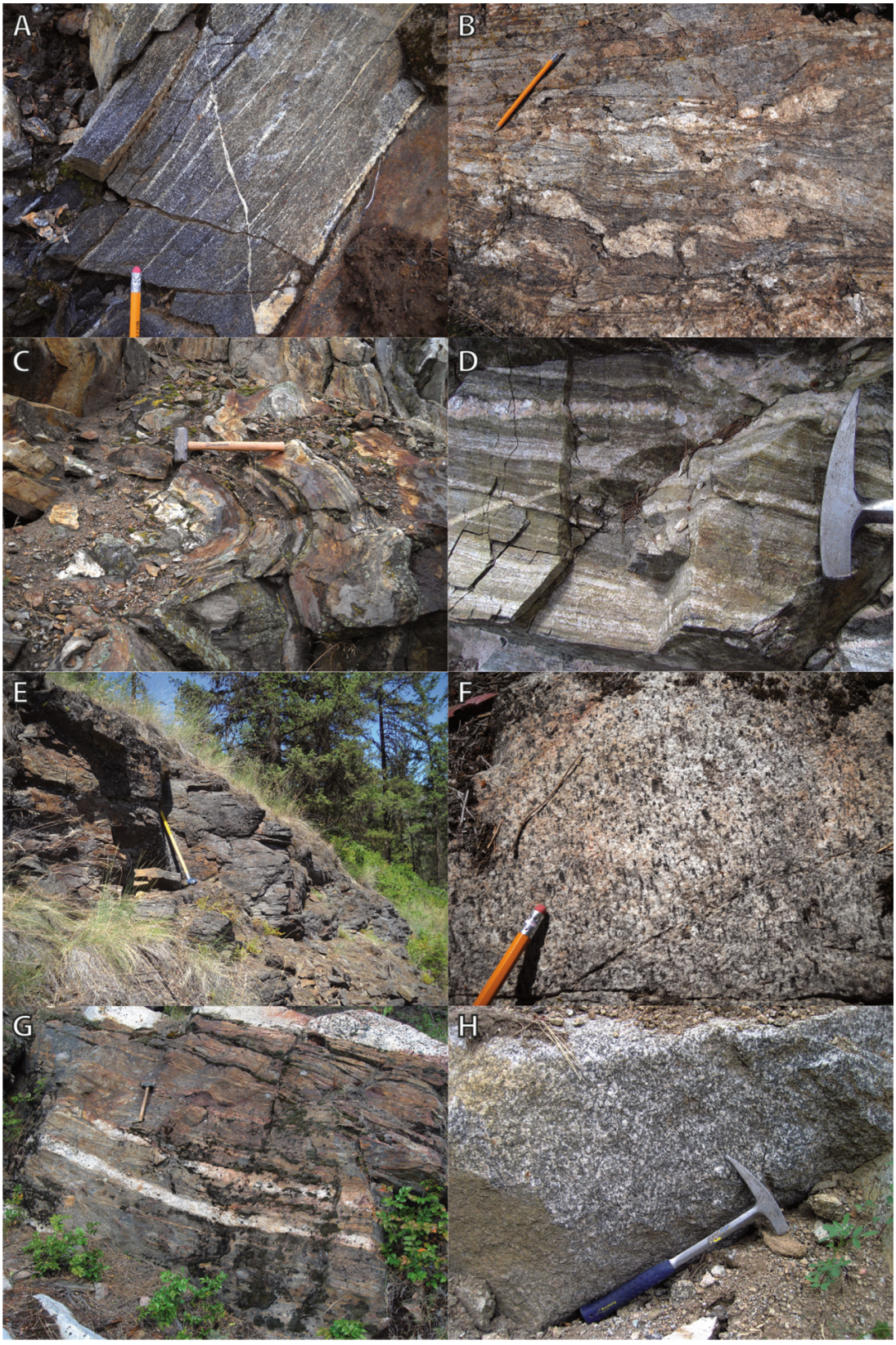

Fig. 4. $^{40}Ar/^{39}Ar$ inverse isotope correlation diagrams and age spectra for GFC hornblende samples: (A) CL353; (B) CL978; (C) CL905; (D) CL1204. The solid black horizontal line is the plateau date. Preferred dates are identified in Table 2. All errors are reported at 2σ levels.

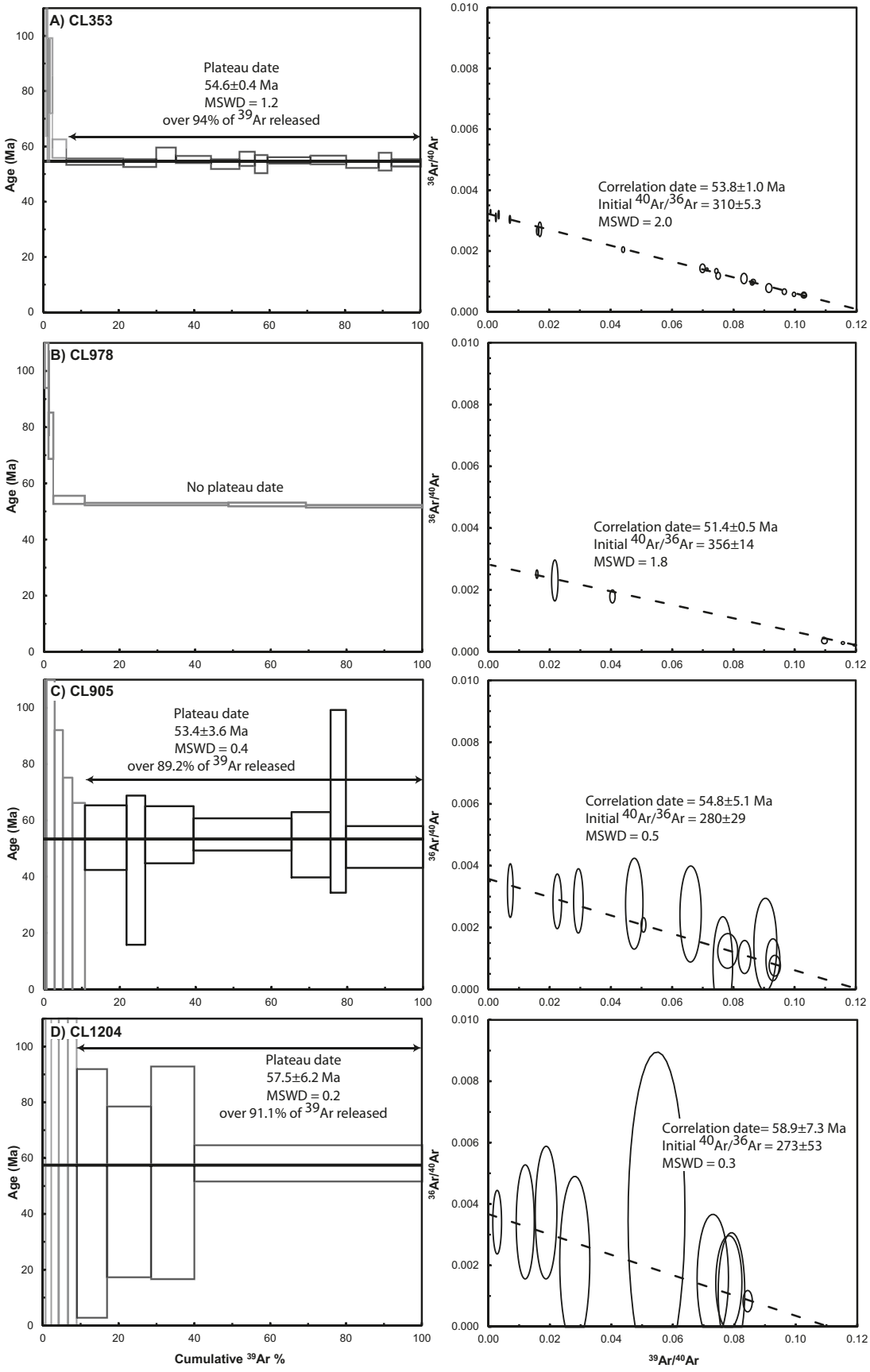

interlayered and locally crosscut by leucocratic bands of 59.5 ± 0.53 Ma (U–Pb zircon) leucogranite interpreted to belong to the Paleocene–Eocene Ladybird suite (Cubley et al. 2013).

KRF apatite samples

Sample CL441 is a fine- to medium-grained, strongly foliated Hbl + Bt tonalite interpreted to belong to the Jurassic Nelson suite. It was collected from the TPSZ, where it exits the north end of Christina Lake and trends northeastward along the Sandner Creek drainage (Fig. 2). Overlying this tonalite is a ~7 m thick layer of nearly undeformed leucogranite and pegmatite interpreted to belong to the Paleocene–Eocene Ladybird suite.

GF hanging wall samples

GF hornblende and biotite samples

Hornblende and biotite grains were analyzed from two granitoid samples correlated with the Jurassic Nelson intrusive suite (CL1201, CL1209). Sample CL1209 is an unfoliated, medium-grained Hbl–Bt granodiorite from the western edge of the National Topographic System (NTS) 082E/01 map sheet, whereas sample CL1201 is an unfoliated to weakly foliated, coarse-grained Hbl–Bt granodiorite that is intruded by a number of Coryell monzonite dikes up to ~10 m wide (Fig. 2). Hornblende and biotite in CL1201 are fresh, with minimal chloritization (Ca/K = 9.5–13.5), but plagioclase is variably sericitized. Late alteration is also observed in CL1209, with sericitization of plagioclase and locally moderate to heavy chloritization of smaller hornblende (Ca/K = 32–45) and biotite grains.

GF apatite samples

Sample GF185 is a coarse-grained Hbl + Bt-syenite collected from a north–south-trending syenite dike in the immediate hanging wall of the GF (Figs. 2, 3H). This syenite is correlated with the 51.1 ± 0.5 Ma Coryell suite (Carr and Parkinson 1989) and is hosted by fine-grained chert of the Carboniferous to Permian Knob Hill Group (Laberge and Pattison 2007).

Analytical methods

$^{40}Ar/^{39}Ar$ analysis

Hornblende and biotite grains were handpicked from sieved and washed bulk separates and then cleaned in an ultrasonic bath. Separated grain sizes typically ranged from 127 to 300 μm, except for fine-grained amphibolites and schists from units Pr4 and Pr5 (60–127 μm). Mineral separates and neutron flux-monitors (standards) were wrapped in Al foil, and the resulting discs were stacked vertically into an 8.5 cm long and 2.0 cm diameter Al irradiation capsule and then irradiated with fast neutrons in position 5C of the McMaster Nuclear Reactor (Hamilton, Ontario) for a duration of 9 h (at 3 MW·h). Packets of flux monitors were located at ca. 1 cm intervals along the irradiation container, and irradiation parameter values, or *J*-values (McDougall and Harrison 1988), for individual samples were determined by second-order polynomial interpolation between replicate analyses of splits for each monitor position in the capsule. Typically the *J*-value varied by <10% over the length of the capsule. No attempt was made to monitor horizontal flux gradients, as these are considered to be minor in the core of the reactor.

All $^{40}Ar/^{39}Ar$ analyses were conducted at the Queen's University laboratory in Kingston, Ontario. For total fusion of neutron flux monitors and laser step-heating, the samples were loaded into pits in a copper sample holder, beneath the ZnS viewport of a small, bakeable stainless steel chamber connected to an ultrahigh vacuum purification system. For step-heating, the laser beam of a 30 W New Wave Research MIR 10-30 CO_2 laser was defocused to 2 mm to cover the entire sample. Three duplicate analyses were done with the same laser fitted with a faceted lens and a 3 mm beam diameter. Heating periods were ca. 3 min at increasing percent power settings (1.5% to 7%). The evolved gas, after purification using an SAES C50 getter (ca. 5 min), was admitted to an online, MAP 216 mass spectrometer, with a Bäur Signer source and an electron multiplier (set to a gain of 100 over the Faraday detector). Blanks, measured routinely, were subtracted from the subsequent sample gas fractions. For masses 40, 39, 37, and 36, the extraction blanks are typically $<10 \times 10^{-13}$, $<0.5 \times 10^{-13}$, $<0.5 \times 10^{-13}$, and $<0.5 \times 10^{-13}$ cm^{-3} at standard temperature and pressure (STP), respectively.

Measured argon-isotope peak heights were extrapolated to zero-time, normalized to the $^{40}Ar/^{36}Ar$ atmospheric ratio (295.5) using measured values of atmospheric argon, and corrected for neutron-induced ^{40}Ar from potassium, ^{39}Ar and ^{36}Ar from calcium, and ^{36}Ar from chlorine (Roddick 1983). Dates and errors were calculated using the procedure of Dalrymple et al. (1981) and the decay constants of Steiger and Jäger (1977). Plateau and inverse isotope correlation dates were calculated using Isoplot version 3.6 (Ludwig 2008). A plateau is defined as three or more contiguous steps containing >50% of the ^{39}Ar released, with a probability of fit >0.01 and a mean square weighted deviates (MSWD) of <2. If the contiguous steps contain <50% of the ^{39}Ar released, it is referred to as a plateau segment. Errors shown in Tables 2 and 3, and on the age spectra and inverse isotope correlation (isochron) diagrams (Figs. 4–8), represent the analytical precision at 2σ, assuming that the error in *J* is zero. This is suitable for comparing within-spectrum variation and determining which steps form a plateau (e.g., McDougall and Harrison 1988). A conservative estimate of this error in the *J*-value is 0.5% and can be added for intersample comparison. The dates and *J*-values for the intralaboratory standard (MAC-83 biotite at 24.36 Ma; Sandeman et al. 1999) are referenced to Taylor Creek Rhyolite (TCR) sanidine at 28.34 Ma and Fish Canyon Tuff (FCT) sanidine at 28.02 Ma (Renne et al. 1998).

Hornblende Ca/K ratios measured on the mass spectrometer were compared with mineral chemistry data obtained on the JEOL JXA-8200 electron microprobe at the University of Calgary. All microprobe analyses were conducted using wavelength dispersive spectrometry, with a current of 20 nA, an accelerating voltage of 15 kV, and a beam size of 5 μm. Hornblende Ca/K ratios were critical in selecting appropriate heating steps and assessing the quality of $^{40}Ar/^{39}Ar$ hornblende measurements. In $^{40}Ar/^{39}Ar$ analyses, Ca/K ratios may be calculated from the $^{37}Ar/^{39}Ar$ ratio and are an effective measure of the homogeneity of the mineral concentrate (de Jong 2009). In hornblende, low Ca/K ratios are tracers of potassic contamination, commonly caused by tiny, intimately intergrown biotite grains (de Jong 2009; Di Vincenzo et al. 2003). For plateau calculations care was taken to choose heating steps with (*i*) constant Ca/K ratios (indicating relatively pure hornblende) and (*ii*) Ca/K ratios close to measured values on the electron microprobe (Appendix 3)[1].

AFT analysis

Apatite samples were prepared for AFT analysis following the standard method of Hurford (1990). Mean ages were obtained using the zeta calibration method (Hurford and Green 1983) with a zeta value of 342.04 ± 19.7, obtained on both Durango and Mont Dromedary apatite standards. Spontaneous fission tracks were etched using 6.5% HNO_3 for 45 s at 20 °C. Induced fission tracks were etched using 40% HF for 40 min at 20 °C. Samples were irradiated at the Oregon State University facility, Oregon, USA. Fission tracks were counted and measured on a Zeiss Axioplan 2 microscope at the CONDATE dating platform at the University of Rennes, France, using a magnification of 1250× under dry objectives. Ages have been calculated using the Trackkey software (Dunkl 2002).

Results

A summary of $^{40}Ar/^{39}Ar$ hornblende and biotite results is given in Tables 2 and 3, respectively. Complete $^{40}Ar/^{39}Ar$ analytical results are presented in Appendices 1 (hornblende) and 2 (biotite)[1],

Table 2. Summary table of $^{40}Ar/^{39}Ar$ hornblende analytical results.

		Preferred age	Inverse isochron method			Plateau date			Integrated date	Ca/K ratios	
Sample	Location	Date	Date	Initial $^{40}Ar/^{36}Ar$ ratio	MSWD	Date	%^{39}Ar released	MSWD	Date	Estimated from $^{37}Ar/^{39}Ar$	Microprobe
CL353	GFC	53.8±1.0	53.8±1.0	310±5.3	2.0	54.6±0.4	94.0	1.2	56.0±0.6	11–12.5	10–12
CL905	GFC	53.4±3.6	54.8±5.1	280±29	0.5	53.4±3.6	89.2	0.4	51.2±4.5	11.5–14	12.5–14.5
CL978	GFC	51.4±0.5	51.4±0.5	356±14	1.8	n/a	n/a	n/a	53.6±0.4	4–6	5.8–7.3
CL1204	GFC	57.5±6.2	58.9±7.3	273±53	0.3	57.5±6.2	91.1	0.2	52.6±11.3	18–22	27–35
CL114	KRF HW	51.7±0.6	51.7±0.6	324±25	0.9	52.3±0.2	76.2	1.6	52.2±0.4	3–6.5	9–10
CL114r	KRF HW	53.2±1.4	53.2±1.4	305±31	0.3	53.1±1.3	77.3	0.9	54.2±2	5–7.5	9–10
CL114/114r combined	KRF HW	51.8±0.6	51.8±0.6	326±25	0.6 (steps 8–15 (114); 18–26 (114r)	52.7±0.3 (all steps)	79.6	0.9	52.7±0.4		9–10
CL1195	KRF HW	51.0±0.7	51.0±0.7	412±41	0.9	52.5±0.2	98.2	1.1	53.0±0.4	6	5.5–6.5
CL1201	GF HW	>131.4±1.0 (max. age step)	n/a	n/a	n/a	n/a	n/a	n/a	117.0±0.9	7.5–9	9.5–13.5
CL1209	GF HW	>149.4±2.1 (max. age step)	n/a	n/a	n/a	n/a	n/a	n/a	124.3±1.3	13–15	32–45
1209r	GF HW	163±6.1	n/a	n/a	n/a	163.0±6.1	52.1	0.6	132.3±4.7	15–20	32–45

Note: Samples are grouped by location in the GFC, KRF hanging wall (KRF HW), and GF hanging wall (GF HW). Uncertainties given at the 2σ level. All plateau and inverse isochron age determinations performed using Isoplot 3.6 (Ludwig 2008). Inverse isochron dates are Model 1 ages that incorporate the respective errors of all data points. The only notable exception to this is the Model 2 age for CL353, which ignores individual data point errors. An entry of "n/a" for inverse isochron method indicates no Model 1 result. The range of calculated Ca/K ratios from $^{40}Ar/^{39}Ar$ analyses are for the plateau or high-*T* steps. Estimated Ca/K ratios equal or approach the microprobe Ca/K ratios, with the exception of CL1209.

Table 3. Summary table of $^{40}Ar/^{39}Ar$ biotite analytical results.

			Inverse isochron method			Plateau and plateau segment dates			Integrated date
Sample	Location	Preferred age	Date	Initial $^{40}Ar/^{36}Ar$ ratio	MSWD	Date	%^{39}Ar released	MSWD	Date
CL347	GFC	51.8±0.5	n/a	n/a	n/a	51.8±0.5**	44.7	0.5	51.7±0.4
CL979	GFC	51.9±0.5	n/a	n/a	n/a	51.9±0.5**	41.8	1	52.2±0.4
CL1207	GFC	51.4±0.2	n/a	n/a	n/a	51.4±0.2*	98.3	1	51.3±0.3
CL1001	GFC	55.6±1.9	55.7±2.6	297±71	0.3	55.6±1.9*	98.2	0.3	54.6±2.3
CL114	KRF HW	52.4±0.3	52.6±0.4	274±11	1.4	52.4±0.3*	89.5	0.9	51.9±0.4
CL114r	KRF HW	51.0±1.0	51.0±1.0	504±97	1.3 (steps 9–15)	53.0±0.6**	33.5	0.6	52.9±0.3
CL114/114r combined	KRF HW	51.2±0.8	51.2±0.8	476±79	1.4 (steps 13–17 (114); 9–15 (114r))	n/a	n/a	n/a	52.5±0.3
CL309	KRF HW	52.3±0.3	n/a	n/a	n/a	54.2±0.3*	60.5	0.4	52.3±0.3
CL1201	GF HW	77.3±0.4	n/a	n/a	n/a	77.3±0.4**	37.3	1.4	75.9±0.4
CL1209	GF HW	89.5±1.1	n/a	n/a	n/a	89.5±1.1**	47.6	1.3	85.9±1.1

Note: Samples are grouped by location in the GFC, KRF hanging wall (KRF HW), and GF hanging wall (GF HW). Uncertainties given at the 2σ level. All plateau and inverse isochron age determinations performed using Isoplot 3.6 (Ludwig 2008). Inverse isochron dates are Model 1 ages that incorporate the respective errors of all data points. An entry of "n/a" for inverse isochron method indicates no Model 1 result.

*Plateau date.

**Plateau segment date.

Fig. 5. $^{40}Ar/^{39}Ar$ age spectra for biotite samples from the GFC: (A) CL347; (B) CL979; (C) CL1207; (D) CL1001. The solid black horizontal line is the plateau or plateau segment date. All errors are reported at 2σ levels.

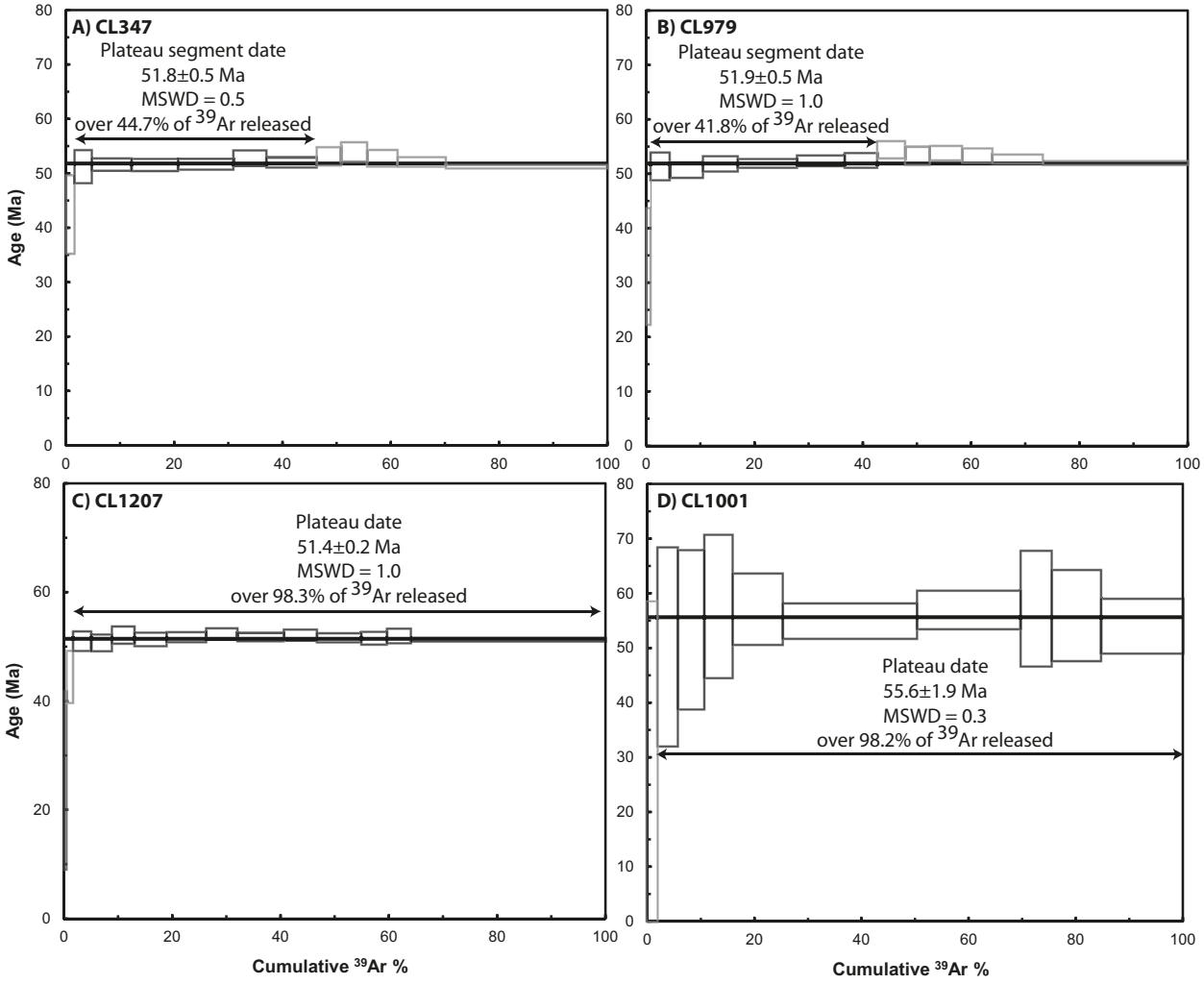

with representative microprobe analyses of hornblende listed in Appendix 3[1]. Petrographic and microprobe analysis shows that some hornblende and biotite grains are partially chloritized, and thus care was taken to identify age steps representative of the unaltered hornblende or biotite.

The partial chloritization of biotite can lead to either saddle- or hump-shaped age profiles that result from an interplay between the differential release of argon from chlorite and biotite during in vacuo heating and ^{39}Ar redistribution by recoil during sample irradiation (Di Vincenzo et al. 2003). ^{39}Ar recoil during irradiation can lead to ^{39}Ar loss in small grains with a high surface area to volume ratio and thus anomalously old ages (Paine et al. 2006). Partial chloritization of biotite and the resulting potassium heterogeneity can amplify these recoil effects, as $^{39}Ar_K$ atoms are expected to recoil from K-rich biotite layers into K-poor chlorite layers (Lo and Onstott 1989; Di Vincenzo et al. 2003). Upon subsequent step-heating, chlorite layers will thus yield anomalously low $^{40}Ar^*/^{39}Ar_K$ ratios ($^{40}Ar^*$ = radiogenic argon) and ages tending to zero, whereas $^{39}Ar_K$-depleted biotite layers will yield anomalously old ages (Di Vincenzo et al. 2003; Paine et al. 2006). Chlorite and biotite possess different thermal release patterns, and during incremental heating the more reactive chlorite degasses at a lower temperature than biotite (Di Vincenzo et al. 2003). Therefore, early low-*T* release steps dominated by chlorite degassing will yield anomalously young ages, while in subsequent medium-*T* steps, biotite already low in $^{39}Ar_K$ owing to argon recoil will yield anomalously old ages. The highest-*T* steps in hump-shaped profiles, illustrating a decrease in apparent ages, could reflect release of argon from progressively larger biotite domains for which $^{39}Ar_K$ recoil loss was less important (Di Vincenzo et al. 2003). Therefore, these highest-*T* steps most likely represent argon release from the least altered biotite (Di Vincenzo et al. 2003).

The largest, least altered grains were chosen for each sample, yet the effects of chloritization and (or) recoil are apparent in a number of age profiles of biotite (e.g., CL979 Bt). Anomalously old dates in the low-*T* steps of some hornblende analyses indicates the presence of excess radiogenic argon, and these steps were not included in the calculation of plateau ages. Excess argon has also been identified as a potential cause for the hump-shaped age profiles described above (Lo and Onstott 1989). Plateau steps that were chosen for age determinations are identified in bold in Appendices 1 and 2[1]. The $^{40}Ar^*/^{39}Ar$ ratio measured for those plateau steps is proportional to the $^{40}Ar^*/^{40}K$ ratio in the sample and therefore proportional to the age at which hornblende or biotite cooled through its argon closure temperature (McDougall and Harrison 1988). This age is referred to as the closure age in the sections that follow.

GFC $^{40}Ar/^{39}Ar$ analyses

Age spectra and inverse isotope correlation (isochron) diagrams are presented for each GFC hornblende sample in Fig. 4, with

Fig. 6. Inverse isotope correlation diagrams and age spectra for hornblende samples from the KRF hanging wall: (A) CL114 Hbl; (B) CL114 Hbl repeat; (C) CL114/CL114 Hbl repeat combination; (D) CL1195 Hbl. The solid black horizontal line is the plateau date. Preferred dates are identified in Table 2. All errors are shown at 2σ levels.

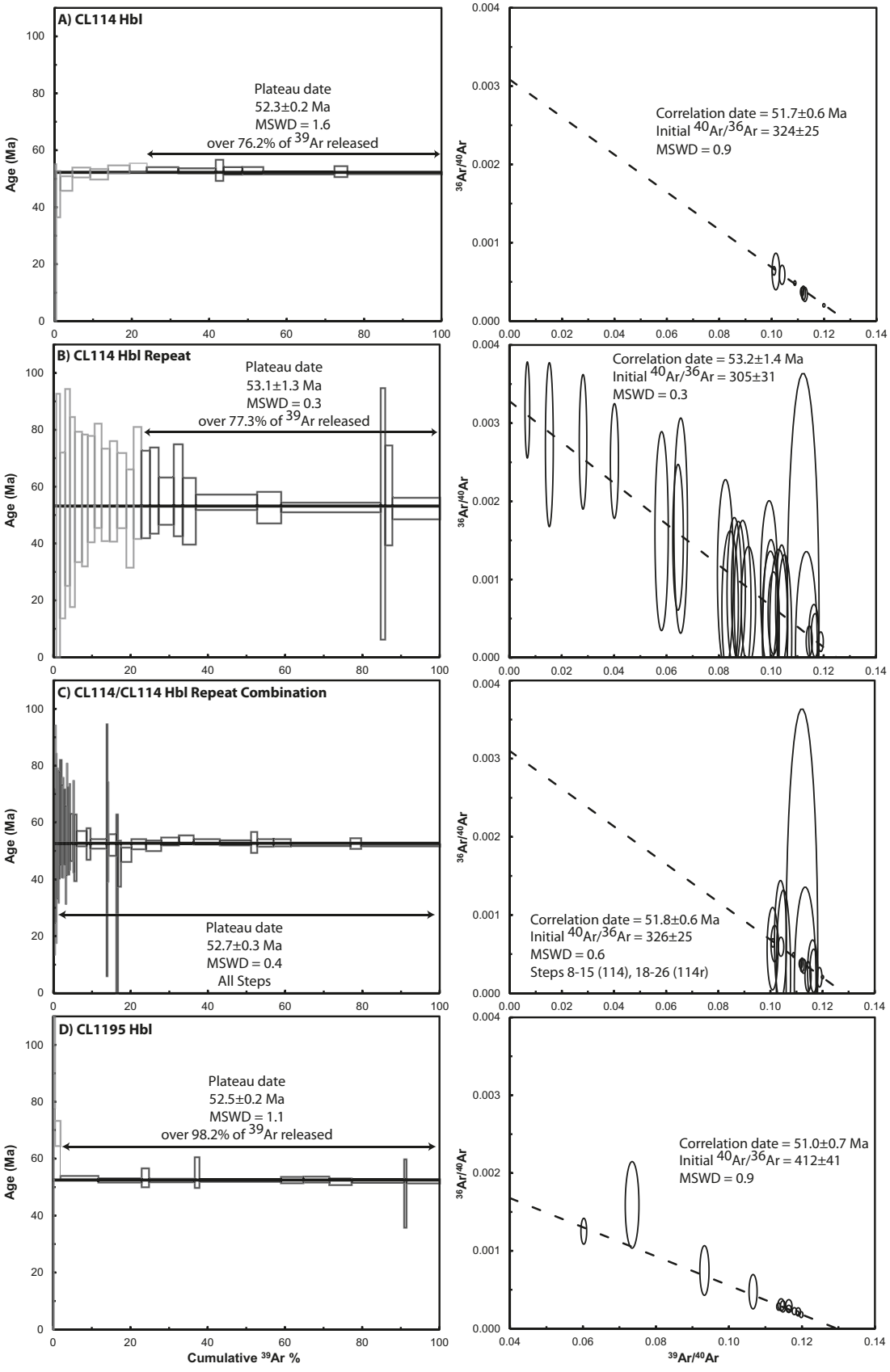

Fig. 7. Inverse isotope correlation diagrams and age spectra for biotite samples from the KRF hanging wall: (A) CL114 Bt; (B) CL114 Bt repeat; (C) CL114/CL114 repeat combination; (D) CL309 Bt. Preferred dates are identified in Table 3. The solid black horizontal line is the plateau or plateau segment date. All errors are shown at 2σ levels.

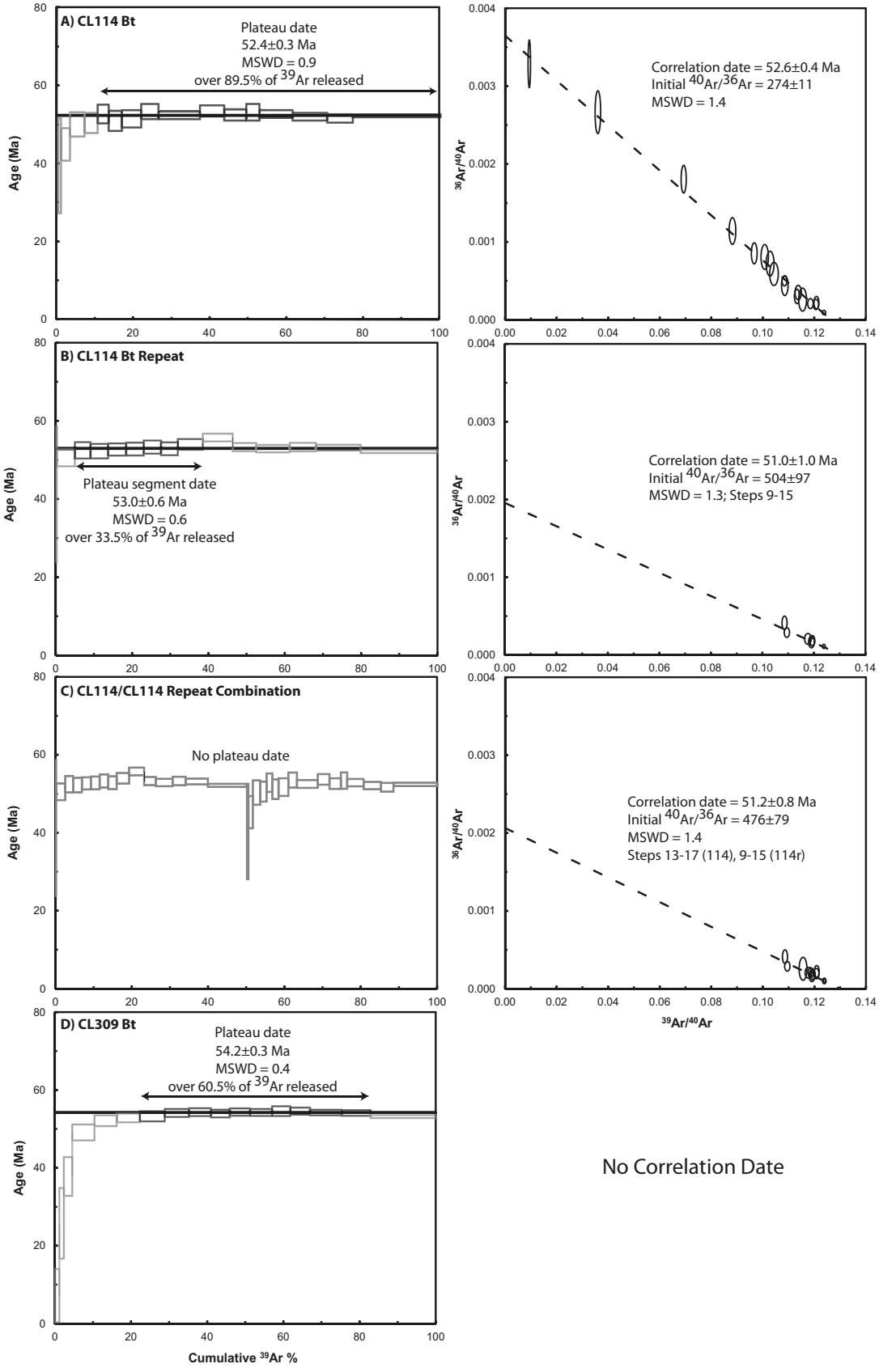

Fig. 8. Age spectra for hornblende and biotite samples from the GF hanging wall: (A) CL1201 Hbl; (B) CL1209 Hbl; (C) CL1209 Hbl repeat; (D) CL1201 Bt; (E) CL1209 Bt. The solid black horizontal line is the plateau or plateau segment date. All errors are shown at 2σ levels.

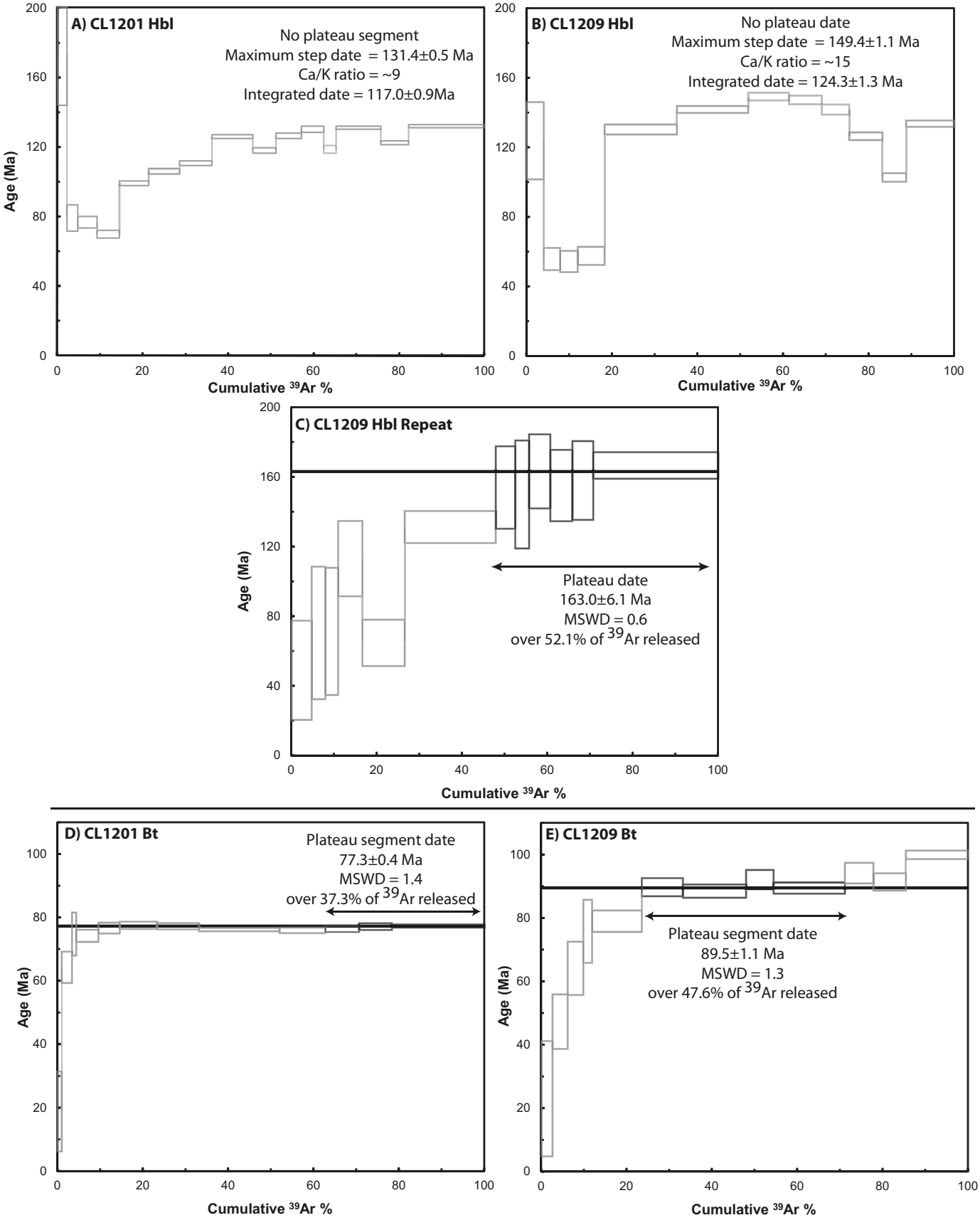

preferred dates identified in Table 2. Sample CL353 yields a plateau date of 54.6 ± 0.4 Ma (MSWD = 1.2), with an overlapping inverse isochron date of 53.8 ± 1.0 (MSWD = 2.0; initial $^{40}Ar/^{36}Ar$ = 310 ± 5.3) (Fig. 4A). Excess argon is suggested by the anomalously old dates in the first few heating steps, but the plateau segment accounts for over 94% of the total argon released. Sample CL978 does not yield a statistical forced plateau date in Isoplot, but the inverse isochron date is 51.4 ± 0.5 Ma (MSWD = 1.8; initial $^{40}Ar/^{36}Ar$ = 356 ± 14) (Fig. 4B). As with CL353, excess argon contamination is suggested by anomalously high initial dates. Error in hornblende analyses is higher for the two fine-grained amphibolite schist samples, CL905 and CL1204. CL905 yields a plateau date of 53.4 ± 3.6 (MSWD = 0.4, 89% ^{39}Ar released) and an overlapping inverse isochron date of 54.8 ± 5.1 Ma (MSWD = 0.5; initial $^{40}Ar/^{36}Ar$ = 280 ± 29), with evidence for excess argon in the first few steps (Fig. 4C). The inconsistent and low Ca/K ratios in the first five steps of the step-heating analysis (Appendix 1)[1] may reflect degassing of K-rich impurities, possibly biotite alteration along grain defects. Partially chloritized hornblende in CL1204 (0.33 wt% K; Appendix 3)[1] yields a plateau date of 57.5 ± 6.2 Ma (MSWD = 0.2; 91% ^{39}Ar released) and an overlapping inverse isochron date of 58.9 ± 7.3 Ma (MSWD = 0.3; initial $^{40}Ar/^{36}Ar$ = 273 ± 53) (Fig. 4D). Owing to the low %K, extent of the alteration, and large error, this date is not considered reliable and is not included in the discussion below.

Age spectra are shown for the four GFC biotite samples in Fig. 5. Correlation diagrams are not shown for biotite samples because most samples return an inverse isochron statistical probability fit of zero when individual errors were considered for all data points (Ludwig 2008) (Table 3). The three paragneiss samples from unit Pr1 (CL347, CL979, CL1207) all yield similar plateau or plateau segment dates: sample CL347 (plateau segment), 51.8 ± 0.5 Ma (MSWD = 0.5; 45% ^{39}Ar released; Fig. 5A); sample CL979 (plateau segment), 51.9 ± 0.5 Ma (MSWD = 1.0; 42% ^{39}Ar released; Fig. 5B); and sample CL1207 (plateau), 51.4 ± 0.2 Ma (MSWD = 1.0; 98% ^{39}Ar released; Fig. 5C). In contrast to CL1207, the age spectra for CL347 and CL979 show slight concave-upwards patterns with humps at intermediate temperatures, possibly reflecting excess argon (Foland 1983; Lo and Onstott 1989) or the effects of ^{39}Ar recoil resulting from chloritization of biotite (McDougall and Harrison 1988; Di Vincenzo et al. 2003; Paine et al. 2006). These spectra have low- to intermediate-*T* plateau segments representing 41%–45% of the total ^{39}Ar released. These segments may be significant (Fig. 5) because the dates are indistinguishable from the highest-*T* steps that are most likely to represent degassing from the least altered domains in the biotite (Di Vincenzo et al. 2003). The fine-grained biotite grains in St + Bt + Sil schist sample CL1001 yield larger errors and an older date, with a plateau at 55.6 ± 1.9 Ma (MSWD = 0.3, 98% of the ^{39}Ar released; Fig. 5D).

KRF and GF hanging wall $^{40}Ar/^{39}Ar$ results

Hornblende and biotite $^{40}Ar/^{39}Ar$ results from the hanging walls to the KRF and GF are shown in Figs. 6–8. Sample CL114 is from a Hbl–Bt granodiorite from the hanging wall of the KRF. Both biotite and hornblende were analyzed in duplicate. The initial analysis of the hornblende yielded a plateau date of 52.3 ± 0.2 Ma (MSWD = 1.6; 76% of the ^{39}Ar released), but the calculated Ca/K ratios (~4, Appendix 1)[1] were erratic and lower than microprobe results (~9; Appendix 3)[1] over the plateau steps. The inverse isochron for the plateau steps (Fig. 6A) yielded a younger date of 51.7 ± 0.6 Ma (MSWD = 1.0; initial $^{40}Ar/^{36}Ar$ = 324 ± 25). The second step-heating analysis of CL114 hornblende was done using modified laser optics on a split from the original irradiation package. More steps were attempted to try to reduce the effect of intergrown minerals in the hornblende. The plateau date for this analysis is 53.1 ± 1.3 Ma (MSWD = 0.3; 77% ^{39}Ar released) (Fig. 6B). The inverse isochron date includes all steps and is 53.2 ± 1.4 Ma (MSWD = 0.3; initial $^{40}Ar/^{36}Ar$ = 305 ± 31). However, taken together the data for the high-*T* and high-Ca/K steps from the two analyses define an inverse isochron date of 51.8 ± 0.6 Ma (MSWD = 0.6; initial $^{40}Ar/^{36}Ar$ = 326 ± 25) (Fig. 6C).

Hornblende grains from the other Nelson suite granodiorite sample, CL1195, yield a plateau date of 52.5 ± 0.2 Ma (MSWD = 1.1; 98% ^{39}Ar released) and an inverse isochron date of 51.0 ± 0.7 Ma (MSWD = 0.9; initial $^{40}Ar/^{36}Ar$ = 412 ± 41; Fig. 6D). The high initial $^{40}Ar/^{36}Ar$ ratio is evidence of a component of excess argon in this hornblende. The first analysis of sample CL114 biotite yielded a plateau date of 52.4 ± 0.3 Ma (MSWD = 0.9; 90% ^{39}Ar released; Fig. 7A), whereas sample CL309 gave an older plateau date of 54.2 ± 0.3 Ma (MSWD = 0.4; 61% ^{39}Ar released; Fig. 7D). Both samples have slight humps in intermediate-*T* steps, suggesting the presence of excess argon and (or) the occurrence of ^{39}Ar recoil. The duplicate analysis of CL114 biotite (Fig. 7B) repeats this pattern but does not yield a plateau date as defined herein. However, the inverse isochron for the seven high-*T* steps (68% ^{39}Ar released) gives a date of 51.0 ± 1.0 Ma (MSWD = 1.3), with an initial $^{40}Ar/^{36}Ar$ ratio of 504 ± 97, and provides further evidence of excess argon in biotite.

Samples in the GF hanging wall yield more complex age spectra recording the earlier Jurassic to Cretaceous cooling history and show evidence for a Late Cretaceous – Eocene thermal disturbance. The spectrum for CL1201 hornblende (Fig. 8A) shows an apparent diffusion loss profile (McDougall and Harrison 1988) with a maximum step date of 131.4 ± 0.5 Ma, indicating that the true age could be >131 Ma. The measured Ca/K ratios for this step, ~9.1, are closest to microprobe data (9.5–13.5). The spectrum for the first analysis of hornblende from sample CL1209 (Fig. 8B) is typical of a multi-phase sample, with a maximum step date of 149 ± 2 Ma. The low-*T* steps probably correspond to intergrown biotite (young dates and low Ca/K ratios) whereas the higher-*T* steps record Ar release from the hornblende. The variation from step to step (in age: 54–149 Ma and Ca/K: 1–17) shows poor separation of the argon released from different phases in this step-heating analysis. A duplicate analysis of a small split from the same irradiation with different laser optics yielded a spectrum that better separates the mixed phases (Fig. 8C). The first step gave a date of 49 ± 20 Ma. Thereafter, step dates climb to a plateau of 163.0 ± 6.1 Ma (MSWD = 0.6; 52% of the ^{39}Ar released). The results for these hornblende samples are consistent with initial cooling and closure of the hornblende Ar system in Middle Jurassic time shortly after emplacement of the pluton (~167 Ma, Cubley et al. 2013). The influence of the Eocene thermal event seems to be on intergrown minerals rather than the hornblende itself.

The spectra for biotite from CL1209 and CL1201 display diffusion loss profiles and yield plateau segment dates of 89.5 ± 1.1 (MSWD = 1.3; 48% ^{39}Ar released) and 77.3 ± 0.4 Ma (MSWD = 1.4, 37% ^{39}Ar released) respectively (Figs. 8D, 8E). The age difference may be due to the proximity of CL1201 to Eocene Coryell dykes in the sampled outcrop. The original cooling age of these biotites cannot be determined from these results.

AFT results

A summary table of AFT results is given in Table 4. The large errors associated with the samples reflect very small apatite grain sizes. The two samples from the GFC, CL315 and GF001B, yield dates of 35.9 ± 6.1 and 34.9 ± 5.4 Ma, respectively. The single sample from the GF hanging wall, GF186, yields a date of 35.1 ± 4.6 Ma, whereas the two samples from the KRF hanging wall, CL114 and CL441, yield dates of 37.2 ± 4.1 and 31.9 ± 3.3 Ma, respectively. The dates for all samples are within error of each other (Fig. 9). A weighted mean average age of the five analyses is 34.6 ± 2.0 Ma (MSWD = 1.2).

Age versus elevation

The $^{40}Ar/^{39}Ar$ and AFT dates from the GFC and KRF hanging wall are shown in Fig. 10, plotted at their respective elevations (metres above sea level). There is no statistical correlation

Table 4. Summary of AFT results.

Sample	Altitude	Nb	$\rho_d \times 10^4$	$\rho_s \times 10^4$	$\rho_i \times 10^4$	[U]	P(χ^2)	Var	FT age	Error (±2σ)
GF001B	472	18	130.2 (9774)	13.26 (57)	84.42 (363)	7.1	100	0.3	34.9	5.4
GF186	944	20	127.8 (9774)	23.74 (94)	147.98 (586)	14.7	32	1.4	35.1	4.6
CL114	624	18	120.3 (9774)	35.37 (139)	194.91 (766)	19.57	99	0.4	37.2	4.1
CL441	974	30	117.8 (9774)	21.38 (155)	134.62 (976)	13.27	5.4	1.6	31.9	3.3
CL315	761	18	112.9 (9774)	15.03 (46)	80.72 (247)	8.6	100	0.4	35.9	6.1

Notes: AFT analysis data. Altitude is the sampling altitude in metres. Nb is the number of crystals analyzed. ρ_d is the CN5 glass dosimeter induced track density per cm^2. Number in brackets is the total number of tracks counted. ρ_S and ρ_i represent sample spontaneous and induced track densities per cm^2. Number in brackets is the total number of tracks counted. [U] is the calculated uranium density (in ppm). P(χ^2) is the probability in % of χ^2 for v degrees of freedom (where v is the number of crystals-1). Var. is the age dispersion in %. FT age is the apatite fission track age in Ma (the pooled age is used when P(χ^2) < 10%, and the central age is used when P(χ^2) > 10%).

between analytical age and elevation for any sample groupings. This conclusion extends to KRF hanging wall AFT samples, whose dates are within error of each other despite a nearly 500 m elevation difference.

Discussion

GFC

The new $^{40}Ar/^{39}Ar$ hornblende data from the GFC demonstrate that the complex passed through hornblende closure temperature between 57.5 and 51.4 Ma. Our results for samples in the central and eastern part of the GFC in the Highway 3 corridor provide tighter constraints between 53.8 ± 1.0 (CL353) and 51.4 ± 0.5 Ma (CL978) (Fig. 4A). The older 57.5 ± 6.2 Ma date from CL1204 is not considered reliable owing to the low %K, extent of the alteration, and large error. The hornblende dates for all GFC samples analyzed in this study are younger than the 64–60 Ma $^{40}Ar/^{40}K$ dates reported by Stevens et al. (1982) and Hunt and Roddick (1990) (Fig. 11). Those older dates were from samples at a stratigraphic level correlative to Pr4 (Fig. 2B) yet are not within analytical error of the new, younger $^{40}Ar/^{39}Ar$ date from Pr4 (sample CL905, 53.4 ± 3.6 Ma). The new date from unit Pr5 (CL1204; 57.5 ± 6.2 Ma) is younger than, but within error of, a single previous $^{40}Ar/^{39}Ar$ hornblende date (59.0 ± 0.2 Ma) from stratigraphically higher amphibolites in unit "eq" in northeastern Washington (Orr and Cheney 1987; Berger and Snee 1992). This unit is not exposed in the field area of this study.

The GFC $^{40}Ar/^{39}Ar$ biotite dates presented in this study are older than, but within error of, earlier published $^{40}Ar/^{40}K$ dates (Fig. 12) (Wanless et al. 1968, 1978; Addie 1980; Stevens et al. 1983; Getty Mines Ltd., unpublished data). Within error, the three samples from the stratigraphically lowest unit (Pr1) yield identical dates, but CL1207 has the best plateau (51.4 ± 0.2 Ma), lacks the intermediate-T age spectrum hump seen in other samples, and is thus interpreted as the closure age. This age is within error of a single $^{40}Ar/^{40}K$ biotite plateau age from an amphibolite in the Kettle dome in Washington State, 51.6 ± 1.4 Ma (Engels et al. 1976).

The data set presented in this study does not reveal any systematic pattern between either $^{40}Ar/^{39}Ar$ hornblende or $^{40}Ar/^{39}Ar$ biotite dates and stratigraphic level within the complex. Hornblende dates from the lowest stratigraphic unit, Pr1 (53.8–51.4 Ma) overlap with dates from overlying units Pr4 and Pr5 (57.5–53.4 Ma) (Fig. 11). Biotite dates from unit Pr1 samples yield younger dates (~52–51.4 Ma) than the single sample from overlying unit Pr5 (CL1001; 55.6 ± 1.9 Ma) (Fig. 12), but the reliability of the latter analysis is questionable owing to its fine grain size and degree of chloritization. The fine grain size and greater chloritization of both hornblende and biotite separates from Pr4 and Pr5 samples may obscure any significant age difference between stratigraphic levels, and a larger data set may ultimately be required to assess changes in cooling ages. A lack of significant age variation between stratigraphic levels suggests that the observed tilting and fault juxtaposition of upper (Pr4, Pr5) and lower (Pr1) units occurred prior to passage of the core complex through hornblende and biotite closure.

A time–temperature (T–t) path for the cooling of the GFC following high-T decompression is shown in Fig. 13, accompanied by a probability-density diagram encompassing all monazite, hornblende, and biotite ages from this study and previous studies in the vicinity of the GFC. It is assumed that hornblende closes to argon loss at 530 ± 30 °C (Harrison 1981) and that argon is lost only through volume diffusion. The closure temperature estimate is based on experiments done on rapidly cooled (>100 °C/Ma) igneous hornblendes. Lower closure temperatures calculated from experiments on metamorphic hornblendes (e.g., Baldwin et al. 1990) were attributed to exsolution lamellae and (or) significant phyllosilicate intergrowths within hornblende, both of which reduce the effective diffusion dimension in hornblende and increase apparent Ar diffusivity. Although all four GFC samples show minor intergrowths of chlorite, the timing of this chloritization relative to hornblende closure is unknown. Lower closure temperatures (435–480 °C) were interpreted for slowly cooled (5 °C/Ma), high-grade amphibolites (e.g., Baldwin et al. 1990; Cosca and O'Nions 1994). Recalculating data from Baldwin et al. (1990) for higher cooling rates (50–100 °C/Ma) yields closure temperatures at or above ~490 °C. A closure temperature estimate of 530 ± 30 °C is preferred, similar to other studies of high-grade amphibolites in the Shuswap complex (e.g., Spear and Parrish 1996; Vanderhaeghe et al. 2003). Lower closure temperatures do not significantly impact the conclusions below. A biotite closure temperature for the T–t path in Fig. 13 is estimated at 280 ± 40 °C, recognizing that similar uncertainties regarding the temperature of isotopic closure exist for biotite as for hornblende (Harrison et al. 1985).

The overlapping hornblende and biotite dates from the GFC are consistent with rapid cooling of the complex in the early Eocene (Fig. 13). Cubley et al. (2013) proposed that 49.9 ± 1.0 Ma monazite growth in the GFC represents the timing of high-T decompression and subsequent leucosome crystallization at temperatures of ~650–735 °C. Laberge and Pattison (2007) also recorded a monazite population at ~50 Ma. These monazite dates overlap with the lower-T hornblende and biotite dates, implying rapid cooling from ~735 to 280 ± 40 °C at ~51 Ma (probability plot, Fig. 13). Cooling rates in excess of 200 °C/Ma are thus implied for the GFC (Fig. 13). The new, younger $^{40}Ar/^{39}Ar$ hornblende dates compared with those of previous studies remove the primary argument for the proposed slow cooling of the GFC following high-T exhumation (Laberge and Pattison 2007).

The observation that a number of $^{40}Ar/^{39}Ar$ hornblende ages are older than the U–Pb monazite ages is problematic and may suggest that the ~50 Ma monazite ages represent crystallization at temperatures lower than hornblende closure, perhaps related to hydrothermal fluid flow. However, based on microtextural observations made in Cubley et al. (2013), we believe this age discrepancy is primarily an analytical artifact. Monazite dates between 52 and 50 Ma are recorded in monazites found in a number of textural locations inherently linked to high-T decompression and subsequent melt crystallization, most notably (*i*) as inclusions in cordierite surrounding sillimanite or garnet, with or without

Fig. 9. (A) GFC AFT dates with associated 2σ errors. All dates, whether from the GFC or hanging wall to the KRF and GF, are within analytical error. A weighted mean average age for all samples is 34.6 ± 2.6 Ma. (B) Probability–density diagram (Isoplot 3.6) of all 56–23 Ma (Eocene–Oligocene) AFT dates recorded in the NTS 082 map sheet in southeastern British Columbia (from Breitsprecher and Mortensen 2003). Gaussian deconvolution highlights two age populations, the younger of which (~33 Ma) is within error of the GFC weighted mean age. See text for details.

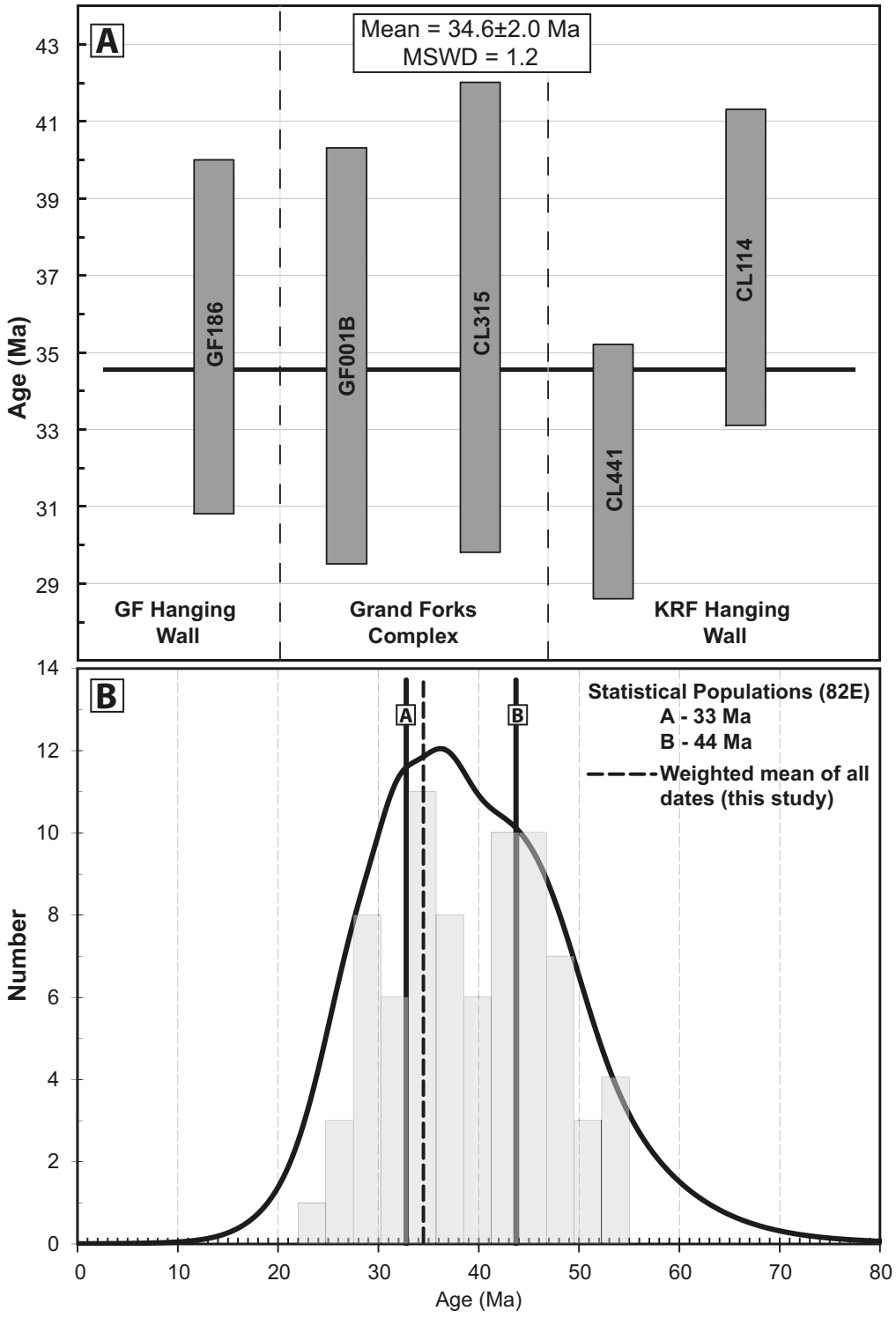

significant pinitization or other evidence for retrograde fluid flow, and (*ii*) as inclusions within large leucosome K-feldspar crystals with no apparent retrograde sericitization. This observation of 52–50 Ma monazite contained as inclusions within unaltered silicate phases differs from the interpretation of Laberge and Pattison (2007) that ~50 Ma monazite growth was limited to matrix grain boundaries and calls into question their interpretation that 50 Ma monazite was related to an intergranular hydrothermal fluid.

The two AFT dates (mean closure temperature ~110 ± 10 °C; Gleadow and Duddy 1981)) from the GFC, 34.9 ± 5.4 and 35.9 ± 6.1 Ma, are within error of each other. The implication is that the

Fig. 10. Elevation versus age diagram for $^{40}Ar/^{39}Ar$ hornblende and biotite plus AFT dates from this study. Errors are reported at 2σ. HW, hanging wall to the Kettle River or Granby fault; FW, footwall (i.e., Grand Forks complex).

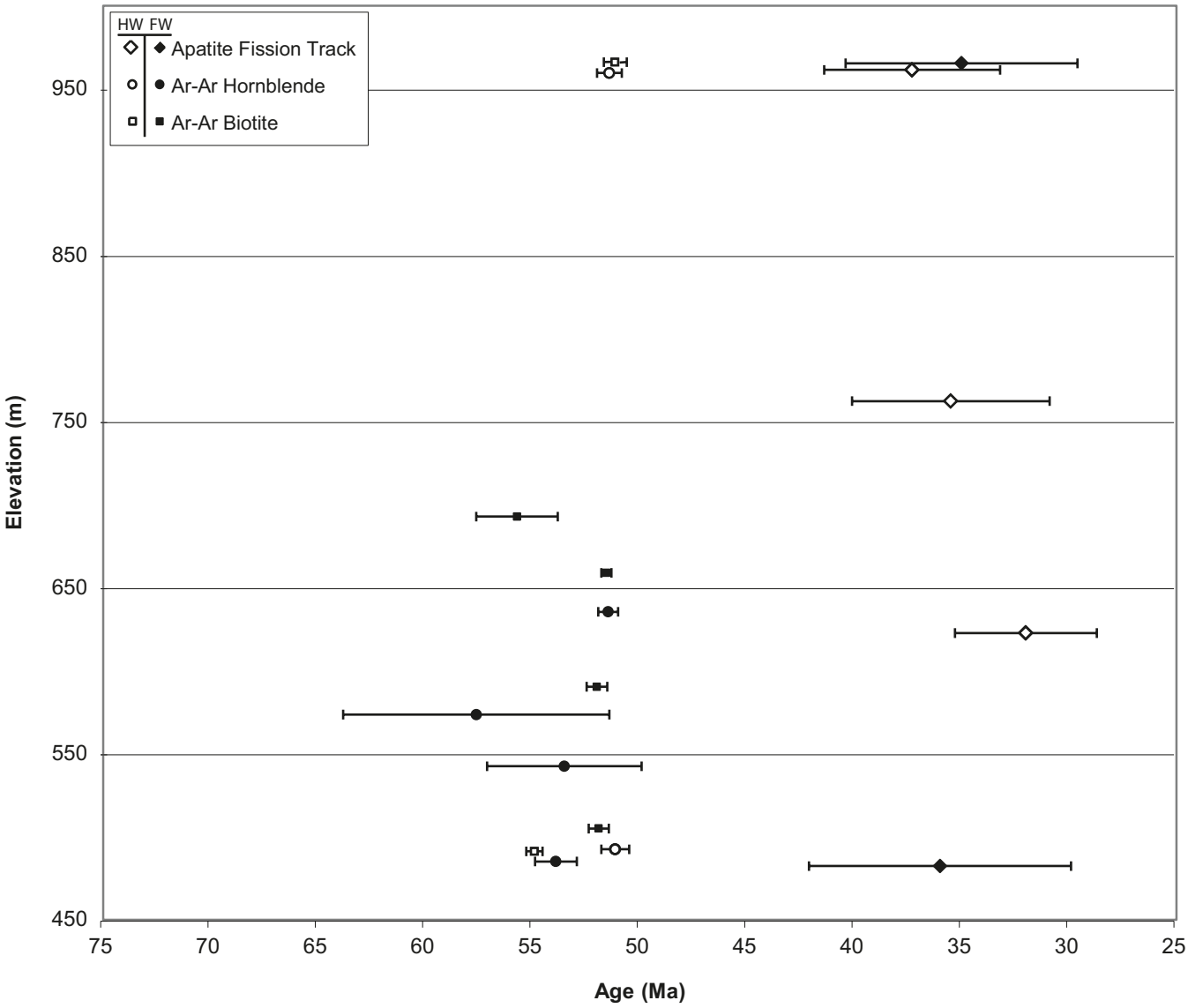

cooling rate dropped from ~200 to ~10 °C/Ma following passage through biotite closure (Fig. 13). A caveat to this interpretation is that variations in annealing kinetics can cause apatite closure temperatures to vary by at least 40 °C (e.g., Kohn and Foster 1996; Ketcham et al. 1999), and thus the exact *T*–*t* path below biotite closure is at best an approximation.

The $^{40}Ar/^{39}Ar$ dates for the GFC agree closely with those found elsewhere in the southern Shuswap complex, most notably the Okanogan dome and Okanagan/Vaseaux gneiss to the west and the Valhalla complex to the east. Recent $^{40}Ar/^{39}Ar$ biotite dating on the Okanogan dome by Kruckenberg et al. (2008) records ages of ~48 Ma. These ages, slightly younger than the ~50 Ma ages in the GFC, may reflect the deeper structural level exposed in the Okanogan dome (9–12 kbar) (Kruckenberg and Whitney 2011) than the GFC (5–6 kbar) (Laberge and Pattison 2007; Cubley and Pattison 2009, 2012). Combining this $^{40}Ar/^{39}Ar$ data with U–Pb zircon data from diatexite, Kruckenberg et al. (2008) proposed cooling from >800 to 325 °C between 51 and 47 Ma, requiring a cooling rate of >100 °C/Ma. The timing and rapid nature of this cooling agrees closely with that now proposed for the GFC (this study).

North of the international border in the Okanagan gneiss, historical $^{40}Ar/^{40}K$ hornblende ages range between 60 and 50 Ma but cluster at ~ 51 Ma, whereas biotite ages range between 53 and 45 Ma but predominantly fall between 50 and 48 Ma (Brown 2010 and references therein). These data require rapid cooling between hornblende and biotite closure similar to that in the Okanogan dome and GFC. East of the GFC in the Valhalla complex, $^{40}Ar/^{40}K$ and $^{40}Ar/^{39}Ar$ data are limited, but new $^{40}Ar/^{39}Ar$ dates from Gordon et al. (2008) suggest passage through hornblende closure at ~55 Ma and biotite closure at 51–48 Ma. These data support older $^{40}Ar/^{40}K$ data that record hornblende closure at 55.5 ± 2.9 Ma and biotite closure at 52.2 ± 2.5 Ma (Wanless et al. 1978, 1979). The overlap of $^{40}Ar/^{39}Ar$ biotite and muscovite ages with U/Th–Pb zircon and monazite ages led Gordon et al. (2009) to propose rapid cooling of the complex between 52 and 48 Ma. Thermal and diffusion modelling of the Valhalla complex by Spear (2004) and Hallett and Spear (2011) suggests a different Valhalla time–temperature path involving rapid cooling (100–200 °C/Ma) of the complex from peak temperatures of 800 °C to <650 °C at

Fig. 11. Comparison of GFC $^{40}Ar/^{39}Ar$ hornblende results from this study (asterisks) with pre-existing $^{40}Ar/^{40}K$ and $^{40}Ar/^{39}Ar$ data. Prior studies: 1, Hunt and Roddick 1990 ($^{40}Ar/^{40}K$); 2, Stevens et al. 1982 ($^{40}Ar/^{40}K$); 3, Berger and Snee 1992 ($^{40}Ar/^{39}Ar$). All errors shown are 2σ. Unit "eq" is a mylonitic quartzite unit not exposed in British Columbia but stratigraphically overlies unit Pr5 in Washington State (Orr and Cheney 1987).

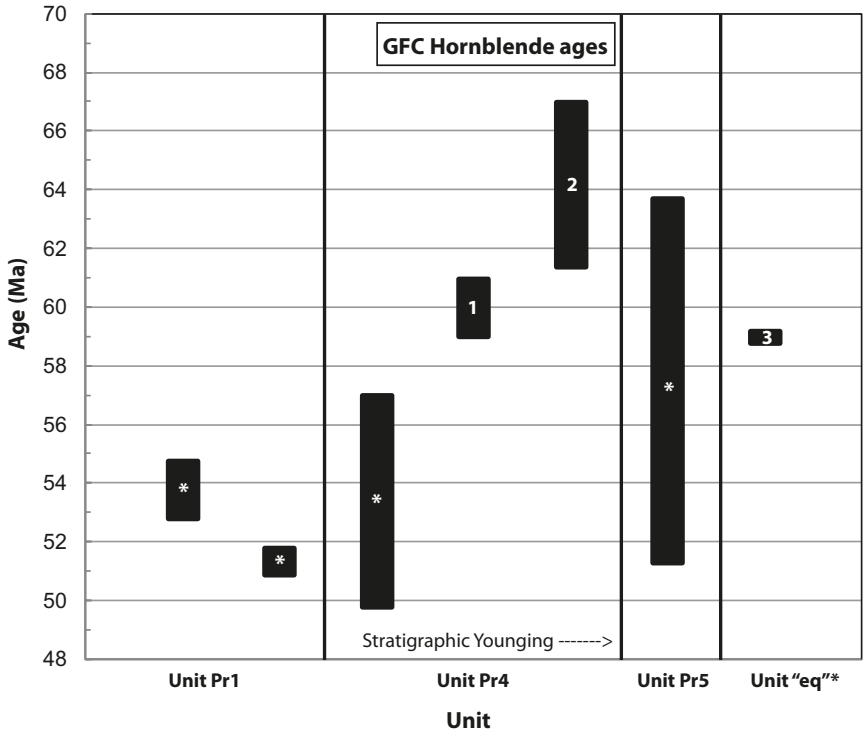

Fig. 12. Comparison of Grand Forks complex (GFC) $^{40}Ar/^{39}Ar$ biotite results from this study (asterisks) with pre-existing $^{40}Ar/^{40}K$ data. Prior studies: 1, Stevens et al. (1983); 2, Wanless et al. (1968); 3, Wanless et al. (1979); 4, Getty Mines Ltd. (unpublished data); 5, Addie (1980). All errors shown are 2σ.

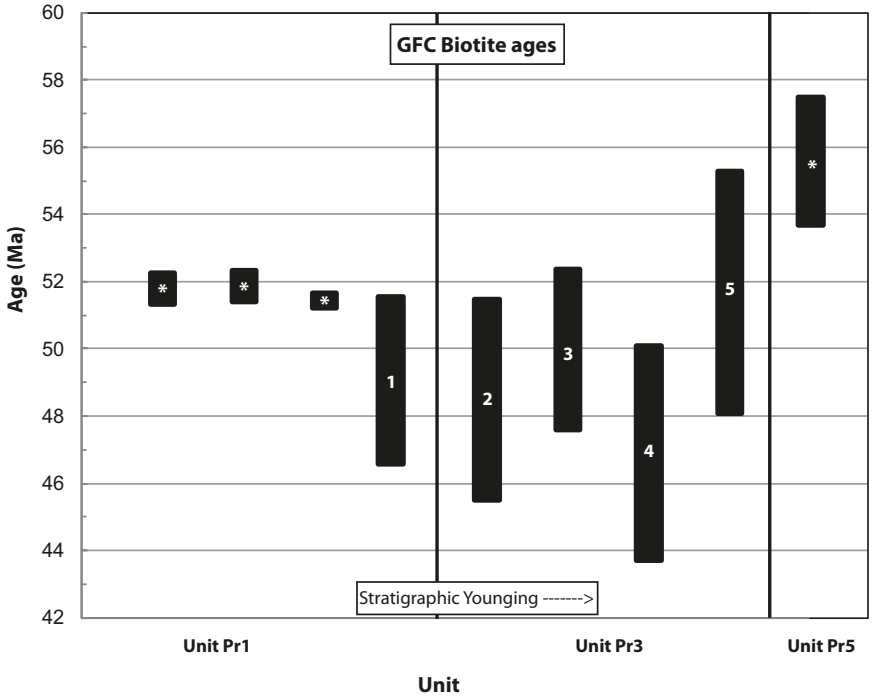

~60–55 Ma. This was followed by a slower cooling rate between the solidus and biotite closure at ~52–48 Ma.

Whereas rapid cooling is inferred in all four areas (GFC, Okanogan dome, Okanagan gneiss, and the Valhalla complex), the absolute timing of this cooling appears to vary, perhaps related to the localized structural mechanisms for exhumation (Hallett and Spear 2011). However, ~52–48 Ma $^{40}Ar/^{40}K$ and $^{40}Ar/^{39}Ar$ biotite ages are consistent across the southern Shuswap complex, suggesting the entire region had achieved similar structural levels and temperature conditions by that time.

Fig. 13. Time–temperature path for Eocene cooling of the GFC. Grey empty boxes are pre-existing geochronological data; black-filled boxes are data from this study. All errors are reported at the 2σ level. Sources for pre-existing data: 1, Cubley et al. (2013); 2, Laberge and Pattison (2007); 3, Stevens et al. (1982); 4, Hunt and Roddick (1990); 5, Wanless et al. (1968); 6, Wanless et al. (1979); 7, Addie (1980); 8, Getty Mines Ltd. (unpublished data). Inset probability–density diagram incorporates $^{40}Ar/^{39}Ar$ or $^{40}Ar/^{40}K$ ages from all hornblende, biotite, or monazite samples, with a highest probability age of 51.4 Ma. Input errors are 1σ. Probability–density plot generated in Isoplot 3.6 (Ludwig 2008).

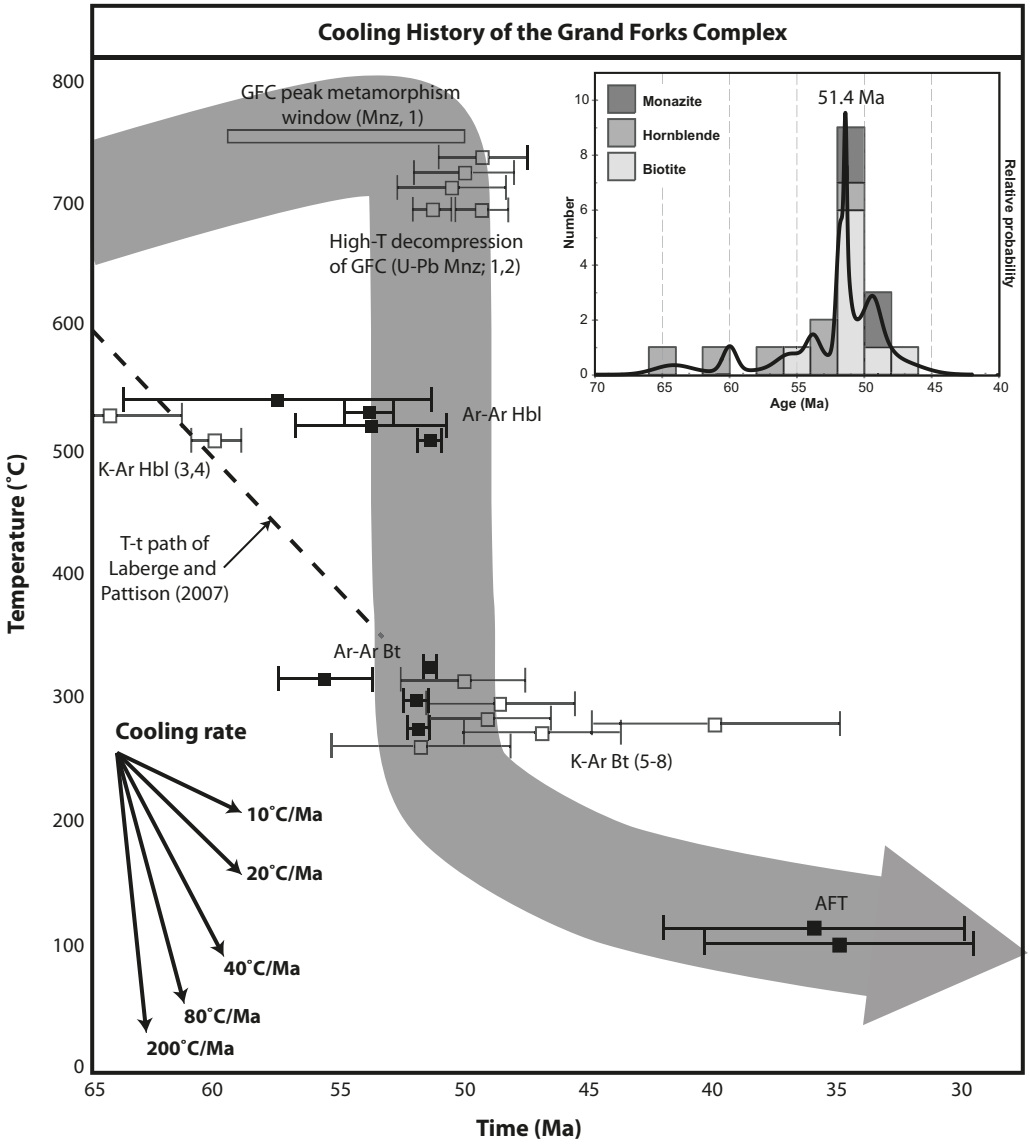

Hanging wall geochronology

The hanging wall rocks to the KRF and GF record a thermal history that is different from that of the underlying GFC. In the hanging wall of the KRF, the combined CL114/CL114r inverse isochron date of 51.8 ± 0.4 Ma (Fig. 6C) is considered to be the best estimate of the time that this rock, and the KRF hanging wall as a whole, cooled below the closure temperature of amphibole during Eocene time. The hornblende inverse isochron dates from CL1195, 51.0 ± 0.7 Ma, and CL114, 51.7 ± 0.4 Ma, closely agree with this estimate. An inverse isochron age of 51.0 ± 1.0 Ma is recorded from the high-*T* steps of biotite analysis CL114r, and this is considered the most reliable estimate of the time at which biotite in the KRF hanging wall cooled below its closure temperature. Generally, Hbl–Bt pairs from this part of the region are characterized by a reverse discordance (biotite date > hornblende date) possibly resulting from incorporation of excess argon into the biotite structure. The overlap between these hornblende and biotite dates suggests rapid cooling of the KRF hanging wall at ~51 Ma. Surprisingly, this rapid cooling in the hanging wall occurred coevally with rapid cooling in the footwall. The relatively flat age profiles and lack of pre-Eocene dates for both hornblende and biotite in the KRF hanging wall are interpreted to reflect near-complete degassing of argon in the early Eocene. The biotite dates from the KRF hanging wall are within error of existing 56–49 Ma $^{40}Ar/^{40}K$ biotite dates from the Coryell batholith east of the GFC (Baadsgaard et al. 1961; Fyles 1984) (Fig. 2B). The overlap between GFC $^{40}Ar/^{39}Ar$ biotite dates (~51 Ma) and KRF hanging wall dates (~51 Ma) suggests that no significant movement occurred on the KRF following passage through biotite closure. Minor movement is evidenced, however, by brittle deformation of 50 Ma granitoid bodies in the KRF fault zone (Cubley et al. 2013).

The dated samples in the hanging wall of the GF do not show the same degree of Eocene resetting observed in the KRF hanging wall. Instead, a Middle Jurassic closure age in hornblende is recorded by a well-defined plateau in one sample. Biotite from the

same rocks have only been partially reset by the Eocene thermal event and still yield dates between 90 and 75 Ma.

A hornblende closure temperature of 530 ± 30 °C is adopted for igneous hornblende grains in hanging wall samples, with the data of Harrison (1981) for rapidly cooled (≥100 °C/Ma) phaneritic intrusives. Samples CL114 and CL1195 in the KRF hanging wall show local intergrowths of chlorite with hornblende in backscattered electron images, with up to 25 μm intergrowths along hornblende cleavage planes. The timing of chloritization is unknown but is likely late. The recalculation of Baldwin et al. (1990) data for chloritized hornblende at higher cooling rates (50–100 °C/Ma) provides a lower closure limit of ~495 °C.

Eocene resetting of $^{40}Ar/^{39}Ar$ ages in the KRF hanging wall is problematic with respect to the presumed timing of peak metamorphism. Numerous authors have proposed that peak regional metamorphism in the KRF hanging wall predated the intrusion of the Nelson suite at 167.9 ± 1.3 Ma (Acton 1998; Acton et al. 2002; Höy 2006; Cubley et al. 2013). Peak temperature conditions for regional metamorphism in the KRF hanging wall are estimated at 440 ± 40 °C (Cubley and Pattison 2012), ~90 °C lower than the hornblende closure temperature of Harrison (1981). In the hanging wall to the GF, peak metamorphism is estimated at 425 ± 40 °C (Laberge and Pattison 2007). Therefore, an Eocene thermal event achieving temperatures >530 °C (Harrison 1981) for an extended time is difficult to explain.

Laberge and Pattison (2007) attributed 50 ± 2 Ma monazite growth in the GFC to thermal or hydrothermal recrystallization related to the emplacement of the Coryell batholith (51.1 ± 0.5 Ma; Carr and Parkinson 1989) and a high regional thermal gradient in the Eocene (Parrish 1995). Although we disagree with this interpretation on textural grounds (see earlier in the text), and the absence of pervasive contact metamorphism associated with the Coryell batholith (Fyles 1984; Stinson 1995; Wilson 1985; Acton 1998; Cubley et al. 2013), its remains possible that thermal effects related to emplacement of the Coryell batholith could be responsible for some degree of Eocene disturbance and (or) resetting of hanging wall $^{40}Ar/^{39}Ar$ hornblende and biotite ages. In the Okanogan Highlands just south of the border in Washington State, Holder and Holder (1988) attributed the thermal degradation of older K–Ar ages to emplacement of the Eocene (50–45 Ma) Colville batholith.

An additional cause of locally elevated hanging wall temperatures in the early Eocene may have been the advection of heat associated with the early high-*T* (~735 °C) decompression stage of GFC exhumation. The importance of this process is a function of the displacement rate of the detachment or detachments accommodating decompression and the fault dip angle, with a shallow dip angle leading to a greater area affected by heat advection (Buck et al. 1988; Dunkl et al. 1998). Whereas several studies have shown that conduction of heat from core complexes into the bounding, overlying hanging wall is sufficient to reset AFT (Foster et al. 1993; Fayon et al. 1996; Dunkl et al. 1998) and muscovite $^{40}Ar/^{39}Ar$ ages (closure T = ~350 °C (Purdy and Jäger 1976)) (van Wees et al. 1992), we are unaware of any studies that propose this for the higher closure temperature of hornblende. Preliminary 1-D heat conduction modelling of the KRF hanging wall following GFC juxtaposition and Coryell batholith emplacement suggests heat input from both sources may have been required to fully reset ages (Cubley 2012).

AFT dates from the KRF and GF hanging walls (~37–32 Ma) overlap with the two GFC ages (~36–35 Ma) (Fig. 9A), implying that no significant movement occurred on the GF or KRF following ~34 Ma. This corroborates the conclusion from $^{40}Ar/^{39}Ar$ biotite dating that suggests insignificant movement on the KRF after 51 Ma. The weighted mean age of all five AFT dates, 34.6 ± 2.0 Ma (Fig. 9A), falls within a widely documented age population in southeastern British Columbia. A probability-density diagram for 55–23 Ma (Eocene–Oligocene) apatite ages recorded in the NTS 082 1:250 000 map sheet is shown in Fig. 9B, based on the compilation of Breitsprecher and Mortensen (2003) and including data from this study and unpublished dates from D. Archibald. Gaussian deconvolution (Ludwig 2008) of this suite of data reveals two age populations at 33 and 44 Ma, with the weighted mean age from this study overlapping with the younger population. In the southern Shuswap complex, the two AFT dates from the GFC are within error of ages from the neighboring Valhalla complex (44–26 Ma; Parrish (1995) and references therein). However, to the west AFT dates from the Okanagan gneiss are ~14 Ma older than those reported in the GFC (mean date = 48.4 Ma; Medford 1975). AFT dates from the GF and KRF hanging walls overlap with a wide range of 45–15 Ma ages from the Nelson batholith in the hanging wall of the Slocan Lake fault on the eastern margin of the Valhalla complex (Sweetkind and Duncan 1989). However, the KRF and GF hanging wall ages are significantly younger than those found in the hanging wall of the Okanagan Valley fault west of the Okanagan gneiss (mean age ~54.3 Ma; Medford 1975).

Acknowledgements

Simon Wing and Mary Samolczyk are thanked for their fieldwork assistance in support of this project. This work was funded by the Natural Sciences and Engineering Research Council (NSERC) Discovery Grant 037233 to D.R.M. Pattison and a contract to J.F. Cubley and D.R.M. Pattison from Targeted Geoscience Initiative 3, Cordilleran Project TG6005 of the Geological Survey of Canada.

References

Acton, S.L. 1998. Geology of the Christina Lake area, B.C. M.Sc. thesis, Department of Geology and Geophysics, University of Calgary, Calgary, Alberta.

Acton, S.L., Simony, P.S., and Heaman, L.M. 2002. Nature of the basement to Quesnel Terrane near Christina Lake, southeastern British Columbia. Canadian Journal of Earth Sciences, **39**(1): 65–78. doi:10.1139/e01-056.

Addie, G.G. 1980. Mineral Property Examinations: Southeast British Columbia, DEB (SD 18). *In* Geological Fieldwork 1979. British Columbia Geological Division, Paper 1980-1, pp. 112–113.

Armstrong, R.L., Parrish, R.R., van derHeyden, P., Scott, K., Runkle, D., and Brown, R.L. 1991. Early Proterozoic basement exposures in the southern Canadian Cordillera; core gneiss of Frenchman Cap, Unit I of the Grand Forks Gneiss, and the Vaseaux Formation. Canadian Journal of Earth Sciences, **28**(8): 1169–1201. doi:10.1139/e91-107.

Baadsgaard, H., Folinsbee, R.E., and Lipson, J.I. 1961. Potassium– argon dates of biotites from Cordilleran granites. Geological Society of America Bulletin, **72**(5): 689–701. doi:10.1130/0016-7606(1961)72[689:PDOBFC]2.0.CO;2.

Baldwin, S.L., Harrison, T.M., and FitzGerald, J.D. 1990. Diffusion of ^{40}Ar in metamorphic hornblende. Contributions to Mineralogy and Petrology, **105**: 691–703. doi:10.1007/BF00306534.

Berger, B.R., and Snee, L.W. 1992. Thermochronologic constraints on mylonite and detachment fault development, Kettle Highlands, northeastern Washington and southern British Columbia. Geological Society of America Abstracts with Programs, **24**: 7.

Breitsprecher, K., and Mortensen, J.K. 2003. Digital compilation of isotopic ages for British Columbia: BC Age 2003 Released as MS-Access Open-File CD. British Columbia Geological Survey Geological Fieldwork, **2003**: 101–104.

Brown, R.L., and Journeay, J.M. 1987. Tectonic denudation of the Shuswap metamorphic terrane of southeastern British Columbia. Geology, **15**(2): 142–146. doi:10.1130/0091-7613(1987)15<142:TDOTSM>2.0.CO;2.

Brown, R.L., and Read, P.B. 1983. Shuswap terrane of British Columbia: a Mesozoic "core complex." Geology, **11**: 164–168.

Brown, S.R. 2010. Geology and geochronology of the southern Okanagan Valley shear zone, southern Canadian Cordillera, British Columbia. Ph.D. thesis, Department of Earth Sciences, Simon Fraser University, Burnaby, British Columbia.

Buck, W.R., Martinez, F., Steckler, M.S., and Cochran, J.R. 1988. Thermal consequences of lithospheric extension: pure and simple. Tectonics, **7**: 213–234. doi:10.1029/TC007i002p00213.

Carr, S.D., and Parkinson, D.L. 1989. Eocene stratigraphy, age of the Coryell Batholith, and extensional faults in the Granby Valley, southern British Columbia. Geological Survey of Canada Paper, **89–1**: 79–87.

Carr, S.D. and Simony, P.S. 2006. Ductile thrusting versus channel flow in the southeastern Canadian Cordillera: evolution of a coherent crystalline thrust sheet. in Law, R.D., Searle, M.P., and Godin, L. (eds.). Channel Flow, Ductile Extrusion, and Exhumation in Continental Collision Zones. Geological Society, London, Special Publications, **268**: 561–587.

Carr, S.D., Parrish, R.R., and Brown, R.L. 1987. Eocene structural development of

the Valhalla complex, southeastern British Columbia. Tectonics, **6**(2): 175–196. doi:10.1029/TC006i002p00175.

Cheney, E.S. 1980. Kettle dome and related structures of northeastern Washington. Geological Society of America Memoir, **153**: 463–483.

Coney, P.J., and Harms, T.A. 1984. Cordilleran metamorphic core complexes: Cenozoic extensional relics of Mesozoic compression. Geology, **12**: 550–554. doi:10.1130/0091-7613(1984)12<550:CMCCCE>2.0.CO;2.

Cosca, M.A., and O'Nions, R.K. 1994. A re-examination of the influence of composition on argon retentivity in metamorphic calcic amphiboles.

Cubley, J.F. 2012. Metamorphism and geochronology of the Grand Forks complex, British Columbia. Ph.D. Thesis, Department of Geoscience, University of Calgary, Calgary, Alberta.

Cubley, J.F., and Pattison, D.R.M. 2009. Metamorphic contrast across the Kettle River fault, southeastern British Columbia: Implications for magnitude of fault displacement. Geological Survey of Canada Current Research Paper, **9**: 1–22.

Cubley, J.F., and Pattison, D.R.M. 2012. Metamorphism and deformation of the Grand Forks complex: implications for the exhumation history of the Shuswap core complex, southern British Columbia. Canadian Journal of Earth Sciences. **49**(11): 1329–1363. doi:10.1139/e2012-066.

Cubley, J.F., Pattison, D.R.M., Tinkham, D.L., and Fanning, C.M. 2013. U–Pb geochronological constraints on the timing of metamorphism and high-T exhumation in the Grand Forks complex, British Columbia. Lithos, v. 156, p. 241–267.

Dalrymple, G.B., Alexander, Jr., E.C., Lanphere, M.A., and Kraker, G.P. 1981. Irradiation of samples for $^{40}Ar/^{39}Ar$ dating using the Geological Survey TRIGA Reactor. U.S. Geological Survey Professional Paper, 1176: 1–55.

deJong, K. 2009. Apparent partial loss $^{40}Ar/^{39}Ar$ age spectra of hornblende from the Palaeoproterozoic Lapland-Kola orogeny (arctic European Russia): insights from numerical modelling and multi-method in-situ micro-sampling geochronology. Geosciences Journal, **13**(3): 317–329. doi:10.1007/s12303-009-0030-4.

DiVincenzo, G., Viti, C., and Rocchi, S. 2003. The effect of chlorite interlayering on ^{40}Ar-^{39}Ar biotite dating: an ^{40}Ar-^{39}Ar laser-probe and TEM investigations of variably chloritised biotites. Contributions to Mineralogy and Petrology, **145**: 643–658. doi:10.1007/s00410-003-0472-z.

Dunkl, I. 2002. TRACKKEY: a Windows program for calculation and graphical presentation of fission track data. Computers and Geosciences, **28**(1): 3–12. doi:10.1016/S0098-3004(01)00024-3.

Dunkl, I., Grasemann, B., and Frisch, W. 1998. Thermal effects of a metamorphic core complex on hanging wall syn-rift sediments: an example from the Rechnitz Window, Eastern Alps. Tectonophysics, **297**: 31–50. doi:10.1016/S0040-1951(98)00162-0.

Engels, J.C., Tabor, R.W., Miller, F.K., and Obradovich, J.D. 1976. Summary of K-Ar, Rb-Sr, U–Pb, Pb(Alpha), and fissiontrack ages of rocks from Washington state prior to 1975 (exclusive of Columbia Plateau basalts). U.S. Geological Survey Miscellaneous Field Studies, Map MF-710.

Erdmer, P., Heaman, L.M., Creaser, R.A., Thompson, R.I., and Daughtry, K.L. 2001. Eocambrian granite clasts in southern British Columbia shed light on Cordilleran hinterland crust. Canadian Journal of Earth Sciences, **38**(7): 1007–1016. doi:10.1139/e01-005.

Fayon, A.K., Stump, E., and Peacock, S.M. 1996. Thermal structure and resetting of apatite fission-track ages in the hanging wall of detachment faults. Abstract Volume of International Workshop on Fission-track Dating, Gent, p. 33.

Foland, K.A. 1983. $^{40}Ar/^{39}Ar$ incremental heating plateaus for biotites with excess argon. Isotope Geoscience, **1**: 3–21.

Foster, D.A., Gleadow, A.J.W., Reynolds, S.J., and Fitzgerald, P.G. 1993. Denudation of metamorphic core complexes and reconstruction of the transition zone, West Central Arizona: Constraints from apatite fission track thermochronology. Journal of Geophysical Research, **98**(B2): 2167–2185. doi:10.1029/92JB02407.

Fyles, J.T. 1990. Geology of the Greenwood-Grand Forks area, British Columbia. British Columbia Ministry of Energy, Mines, and Petroleum Resources Open File Report, **1990-25**: 1–19.

Fyles, J.T. , 1984. Geological setting of the Rossland mining camp. British Columbia Ministry of Energy, Mines and Petroleum Resources Bulletin, **74**: 1–61.

Gessner, K., Wijns, C., and Moresi, L. 2007. Significance of strain localization in the lower crust for the structural evolution and thermal history of metamorphic core complexes. Tectonics, **26**: TC2012. doi:10.1029/2004TC001768.

Gibson, H.D., Brown, R.L., and Parrish, R.R. 1999. Deformation-induced inverted metamorphic field gradients: an example from the southeastern Canadian Cordillera. Journal of Structural Geology, **21**(7): 751–767. doi:10.1016/S0191-8141(99)00051-6.

Gleadow, A.J.W., and Duddy, I.R. 1981. A natural long-term track annealing experiment for apatite. Nuclear Tracks and Radiation Measurements, **5**: 169–174.

Glombick, P., Thompson, R.I., Erdmer, P., Heaman, L., Friedman, R.M., Villeneuve, M., and Daughtry, K.L. 2006. U–Pb constraints on the thermotectonic evolution of the Vernon antiform and the age of the Aberdeen gneiss complex, southeastern Canadian Cordillera. Canadian Journal of Earth Sciences, **43**(2): 213–244. doi:10.1139/e05-096.

Gordon, S.M., Whitney, D.L., Teyssier, C., Grove, M., and Dunlap, W.J. 2008. Timescales of migmatization, melt crystallization, and cooling in a Cordilleran gneiss dome: Valhalla complex, southeastern British Columbia. Tectonics, **27**: 1–28.

Gordon, S.M., Grove, M., Whitney, D.L., Schmitt, A.K., and Teyssier, C. 2009. Time-temperature-fluid evolution of migmatite dome crystallization: Coupled U–Pb age, Ti thermometry, and O isotopic ion microprobe depth profile of zircon and monazite. Chemical Geology, **262**: 186–201. doi:10.1016/j.chemgeo.2009.01.018.

Hallett, B.W., and Spear, F.S. 2011. Insight into the cooling history of the Valhalla complex, British Columbia. Lithos, **125**: 809–824. doi:10.1016/j.lithos.2011.05.002.

Harrison, T.M. 1981. Diffusion of ^{40}Ar in hornblende. Contributions to Mineralogy and Petrology, **78**(3): 324–331.

Harrison, T.M., Duncan, I., and McDougall, I. 1985. Diffusion of ^{40}Ar in biotite; temperature, pressure and compositional effects. Geochimica et Cosmochimica Acta, **49**(11): 2461–2468. doi:10.1016/0016-7037(85)90246-7.

Hinchey, A.M., Carr, S.D., McNeill, P.D., and Rayner, N. 2006. Paleocene–Eocene high-grade metamorphism, anatexis, and deformation in the Thor–Odin dome, Monashee complex, southeastern British Columbia. Canadian Journal of Earth Sciences, **43**(9): 1341–1365. doi:10.1139/e06-028.

Hinchey, A.M., Carr, S.D., and Rayner, N. 2007. Bulk compositional controls on the preservation of age domains within metamorphic monazite: A case study from quartzite and garnet-cordierite-gedrite gneiss of Thor-Odin dome, Monashee complex, Canadian Cordillera. Chemical Geology, **240**: 85–102. doi:10.1016/j.chemgeo.2007.02.001.

Holder, R.W., and Holder, G.A. 1988. The Colville batholith: Tertiary plutonism in northeast Washington associated with graben and core-complex (gneiss dome) formation. Geological Society of America Bulletin, **100**: 1971–1980.

Höy, T. 2006. Geology of the Hope 1 claim, Christina Lake area, southeastern British Columbia. Fieldwork report for Kootenay Gold Inc., Greenwood mining district, 13p. Available from: http://aris.empr.gov.bc.ca/ArisReports/29122.PDF [Accessed 2 February 2012.].

Höy, T., and Jackaman, W. 2005*a*. Geology and Mineral Potential of the Grand Forks Map Sheet (082E/01), Southeastern British Columbia. British Columbia Geological Survey Geological Fieldwork, **2005-1**: 225–230.

Höy, T., and Jackaman, W. 2005*b*. Geology of the Grand Forks Map Sheet (082E/01). British Columbia Ministry of Energy and Mines Geoscience Map 2005-2, scale 1:50,000.

Hunt, P.A., and Roddick, J.C. 1990. A compilation of K–Ar ages; report 19. *in* Radiogenic age and isotopic studies, Report 3. Geological Survey of Canada Paper, **89–02**: 153–190.

Hurford, A.J. 1990. Standardization of fission track dating calibration: Recommendation by the Fission Track Working Group of the I.U.G.S. Subcommission on Geochronology. Chemical Geology (Isotope Geoscience Section), **80**: 171–178.

Hurford, A.J., and Green, P.F. 1983. The zeta age calibration of fission-track dating. Chemical Geology, **1**: 285–317.

Johnson, B.J., and Brown, R.L. 1996. Crustal structure and early Tertiary extensional tectonics of the Omineca belt at 51°N latitude, southern Canadian Cordillera. Canadian Journal of Earth Sciences, **33**(12): 1596–1611. doi:10.1139/e96-121.

Ketcham, R.A., Donelick, R.A., and Carlson, W.D. 1999. Variability of apatite fission-track annealing kinetics III: Extrapolation to geologic time scales. American Mineralogist, **84**: 1235–1255.

Kohn, B.L., and Foster, D.A. 1996. Exceptional chlorine variation in the Stillwater complex, Montana: Thermochronological consequences. International Workshop on Fission-Track Dating, **37**, Ghent.

Kretz, R. 1983. Symbols for rock-forming minerals. American Mineralogist, **68** (1–2): 277–279.

Kruckenberg, S.C., and Whitney, D.L. 2011. Metamorphic evolution of sapphirine- and orthoamphibole-cordierite-bearing gneiss, Okanogan dome, Washington, USA. Journal of Metamorphic Geology, **29**(4): 425–449. doi:10.1111/j.1525-1314.2010.00926.x.

Kruckenberg, S.C., Whitney, D.L., Teyssier, C., Fanning, C.M., and Dunlap, W.J. 2008. Paleocene-Eocene migmatite crystallization, extension, and exhumation in the hinterland of the northern Cordillera: Okanogan dome, Washington, USA. Geological Society of America Bulletin, **120**(7): 1–25.

Laberge, J.D. 2005. Geology of the Granby Fault, southeastern British Columbia: metamorphism and tectonic evolution. M.Sc. thesis, Department of Geology and Geophysics, University of Calgary, Calgary, Alberta. 261p.

Laberge, J.D., and Pattison, D.R.M. 2007. Geology of the western margin of the Grand Forks complex, southern British Columbia: high-grade Cretaceous metamorphism followed by early Tertiary extension on the Granby fault. Canadian Journal of Earth Sciences, **44**(2): 199–228. doi:10.1139/e06-101.

Lo, C.H., and Onstott, T.C. 1989. ^{39}Ar recoil artefacts in chloritized biotite. Geochimica et Cosmochimica Acta, **53**: 2697–2711. doi:10.1016/0016-7037(89)90141-5.

Lorencak, M., Seward, D., Vanderhaeghe, O., Teyssier, C., and Burg, J.P. 2001. Low-temperature cooling history of the Shuswap metamorphic core complex, British Columbia: constraints from apatite and zircon fission-track ages. Canadian Journal of Earth Sciences, **38**(11): 1615–1625. doi:10.1139/e01-037.

Ludwig, K.R. 2008. User's Manual for ISOPLOT 3.6 - A Geochronological Toolkit for Microsoft Excel. Berkeley Geochronological Centre Special Publication Number 4, 77 pp.

Malavieille, J. 2010. Impact of erosion, sedimentation, and structural heritage on the structure and kinematics of orogenic wedges: Analog models and case studies. GSA Today, **20**(1): 4–10. doi:10.1130/GSATG48A.1.

McDougall, I., and Harrison, T.M. 1988. Geochronology and Thermochronology by the $^{40}Ar/^{39}Ar$ Method. Oxford University Press, New York. 212 p.

Medford, G.A. 1975. K–Ar and fission track geochronometry of an Eocene thermal event in the Kettle River (West Half) map area, southern British Columbia. Canadian Journal of Earth Sciences, **12**(5): 836–843. doi:10.1139/e75-072.

Monger, J.W.H., Price, R.A., and Tempelman-Kluit, D.J. 1982. Tectonic accretion and the origin of the two major metamorphic and plutonic welts in the Canadian Cordillera. Geology, **10**: 70–75. doi:10.1130/0091-7613(1982)10<70:TAATOO>2.0.CO;2.

Mulch, A., Teyssier, C., Cosca, M.A., and Chamberlain, C.P. 2007. Stable isotope paleoaltimetry of Eocene core complexes in the North American Cordillera. Tectonics, **26**(4): 1–13.

Norlander, B.H., Whitney, D.L., Teyssier, C., and Vanderhaeghe, O. 2002. Partial melting and decompression of the Thor-Odin Dome, Shuswap metamorphic core complex, Canadian Cordillera. Lithos, **61**: 103–125. doi:10.1016/S0024-4937(02)00075-0.

Okulitch, A.V. 1984. The role of the Shuswap Metamorphic Complex in Cordilleran tectonism: a review. Canadian Journal of Earth Sciences, **21**(10): 1171–1193. doi:10.1139/e84-123.

Orr, K.E., and Cheney, E.S. 1987. Kettle and Okanogan Domes, Northeastern Washington and Southern British Columbia. Washington Division of Geology and Earth Resources Bulletin, **77**: 55–72.

Paine, J.H., Nomade, S., and Renne, P.R. 2006. Quantification of ^{39}Ar recoil ejection from GA1550 biotite during neutron irradiation as a function of grain dimensions. Geochimica et Cosmochimica Acta, **70**: 1507–1517. doi:10.1016/j.gca.2005.11.012.

Parrish, R.R. 1995. Thermal evolution of the southeastern Canadian Cordillera. Canadian Journal of Earth Sciences, **32**(10): 1618–1642. doi:10.1139/e95-130.

Parrish, R.R., Carr, S.D., and Parkinson, D.L. 1988. Eocene Extensional Tectonics and Geochronology of the Southern Omineca Belt, British Columbia and Washington. Tectonics, **7**(2): 181–212. doi:10.1029/TC007i002p00181.

Pigage, L.C. 1977. Rb–Sr dates for granodiorite intrusions on the northeast margin of the Shuswap Metamorphic Complex, Cariboo Mountains, British Columbia. Canadian Journal of Earth Sciences, **14**(7): 1690–1695. doi:10.1139/e77-144.

Preto, V.A.G. 1970. Structure and petrology of the Grand Forks Group, British Columbia. Geological Survey of Canada Paper, **69-2**: 1–80.

Purdy, J.W., and Jäger, E. 1976. K-Ar ages on rock-forming minerals from the Central Alps. Mem. Ist. Geol. Min. Univ. Padov, **30**: 31p.

Renne, P.R., Swisher, C.C., Deino, A.L., Karner, D.B., Owens, T.L., and DePaolo, D.J. 1998. Intercalibration of standards, absolute ages and uncertainties in 40Ar/39Ar dating. Chemical Geology, **145**: 117–152. doi:10.1016/S0009-2541(97)00159-9.

Rey, P.F., Teyssier, C., and Whitney, D.L. 2009. Extension rates, crustal melting, and core complex dynamics. Geology, **37**(5): 391–394. doi:10.1130/G25460A.1.

Rhodes, B.P, and Cheney, E.S. 1981. Low-angle faulting and origin of the Kettle dome, a metamorphic core complex in northeastern Washington. Geology, **9**(8): 366–369. doi:10.1130/0091-7613(1981)9<366:LFATOO>2.0.CO;2.

Roddick, J.C. 1983. High precision intercalibration of $^{40}Ar/^{39}Ar$ standards. Geochimica et Cosmochimica Acta, **47**: 887–898. doi:10.1016/0016-7037(83)90154-0.

Ross, M., and Parrish, R.R. 1991. Detrital zircon geochronology of metasedimentary rocks in the southern Omineca Belt, Canadian Cordillera. Canadian Journal of Earth Sciences, **28**(8): 1254–1270. doi:10.1139/e91-112.

Sandeman, H.A., Archibald, D.A., Grant, J.W., Villeneuve, M.E., and Ford, F.D. 1999. Characterization of the chemical composition and $^{40}Ar/^{39}Ar$ systematics of intralaboratory standard MAC-83 biotite. *in* Radiogenic Age and Isotopic Studies: Report 12; Geological Survey of Canada Current Research, **1999-F**: 13–26.

Schaubs, P.M., Carr, S.D., and Berman, R.G. 2002. Structural and metamorphic constraints on ca. 70 Ma deformation of the northern Valhalla complex, British Columbia: implications for the tectonic evolution of the southern Omineca belt. Journal of Structural Geology, **24**: 1195–1214.

Simony, P.S., and Carr, S.D. 1997. Large lateral ramps in the Eocene Valkyr shear zone: extensional ductile faulting controlled by plutonism in southern British Columbia. Journal of Structural Geology, **19**(6): 769–784. doi:10.1016/S0191-8141(97)00011-4.

Simony, P.S., and Carr, S.D. 2011. Cretaceous to Eocene Evolution of the Southeastern Canadian Cordillera: Continuity of Rocky Mountain Thrust Systems with Zones of 'In-Sequence' Mid-Crustal Flow. Journal of Structural Geology, **33**: 417–434.

Spear, F.S. 2004. Fast Cooling and Exhumation of the Valhalla Metamorphic Core Complex, Southeastern British Columbia. International Geology Review, **46**(3): 193–209. doi:10.2747/0020-6814.46.3.193.

Spear, F.S., and Parrish, R.R. 1996. Petrology and cooling rates of the Valhalla complex, British Columbia, Canada. Journal of Petrology, **37**(4): 733–765. doi:10.1093/petrology/37.4.733.

Steiger, R.H., and Jäger, E. 1977. Subcommission on geochronology: Convention on the use of decay constants in geo- and cosmo-chronology. Earth and Planetary Science Letters, **36**: 359–362. doi:10.1016/0012-821X(77)90060-7.

Stevens, R.D., Delabio, R.N., and Lachance, G.R. 1982. Age determinations and geological studies, K–Ar isotopic ages, Report 15. Geological Survey of Canada Paper 81–2.

Stevens, R.D., Delabio, R.N., and Lachance, G.R. 1983. Age determinations and geological studies; K–Ar isotopic ages, Report 16. Geological Survey of Canada, Paper 82–2.

Stinson, P.K., 1995. Emplacement of the Coryell Batholith. M.Sc. thesis, Department of Geology and Geophysics, University of Calgary, Calgary, Alberta.

Suydam, J.D., and Gaylord, D.R. 1997. Toroda Creek half graben, northeast Washington: Late-stage sedimentary infilling of a synextensional basin. Geological Society of America Bulletin, **109**(10): 1333–1348. doi:10.1130/0016-7606(1997)109<1333:TCHGNW>2.3.CO;2.

Sweetkind, D.S., and Duncan, I.J. 1989. Fission-track evidence for Cenozoic uplift of the Nelson batholith, southeastern British Columbia. Canadian Journal of Earth Sciences, **26**(10): 1944–1952. doi:10.1139/e89-164.

Tempelman-Kluit, D.J. 1999. Geology, Penticton, British Columbia. Geological Survey of Canada Map 1736A, scale 1:250,000.

Teyssier, C., Ferré, E., Whitney, D.L., Norlander, B.H., Vanderhaeghe, O., and Parkinson, D.L. 2005. Flow of partially molten crust and origin of detachments during collapse of the Cordilleran Orogen. *In* High-strain Zones: Structures and Physical Properties. *Edited by* D. Bruhn and L. Burlini. Geological Society of London Special Publication, **245**: 39–64.

Unterschutz, J.L.E, Creaser, R.A., Thompson, R.I., and Daughtry, K.L. 2002. North American margin origin of Quesnel terrane strata in the southern Canadian Cordillera: Inferences from geochemical and Nd isotopic characteristics of Triassic metasedimentary rocks. Geological Society of America Bulletin, **114**(4): 462–475. doi:10.1130/0016-7606(2002)114<0462:NAMOOQ>2.0.CO;2.

vanWees, J.D., de, Jong, K., and Cloetingh, S. 1992. Two-dimensional P-T-t modeling and the dynamics of extension and inversion in the Beltic Zone (SE Spain). Tectonophysics, **203**: 305–324. doi:10.1016/0040-1951(92)90229-Y.

Vanderhaeghe, O., Teyssier, C., McDougall, I., and Dunlap, W.J. 2003. Cooling and exhumation of the Shuswap Metamorphic Core Complex constrained by $^{40}Ar/^{39}Ar$ thermochronology. Geological Society of America Bulletin, **115**: 200–216. doi:10.1130/0016-7606(2003)115<0200:CAEOTS>2.0.CO;2.

Wanless, R.K., Stevens, R.D., Lachance, G.R., and Edmonds, C.M. 1968. Age determinations and geological studies; K–Ar isotopic ages, Report 8. Geological Survey of Canada, Paper 67-2a.

Wanless, R.K., Stevens, R.D., Lachance, G.R., and Delabio, R.N. 1978. Age determinations and geological studies, K-Ar isotopic ages: Report 13. Geological Survey of Canada, Paper 78-2.

Wanless, R.K., Stevens, R.D., Lachance, G.R., and Delabio, R.N. 1979. Age determinations and geological studies; K–Ar isotopic ages; Report 14. Geological Survey of Canada, Paper 79-2.

Wheeler, J.O., and McFeely, P. 1991. Tectonic assemblage map of the Canadian Cordillera and adjacent parts of the United States of America. Geological Survey of Canada Map 1712A, scale 1: 2,000,000.

Wilson, G.L. 1985. Geological, geochemical and prospecting report; Joy 1-4 mineral claims. Fieldwork report for Rex Silver Mines, Ltd., 18p. Available from: http://aris.empr.gov.bc.ca/ArisReports/12367.PDF [Accessed 2 February 2012].